Automated Design Optimization for Hypersonic Plasma-Aerodynamics

Phase-I STTR Contract # FA9550-04-C-0117

Final Phase-I Progress Report, June 2005

by

Ramakanth Munipalli*, Kamesh Subbarao⊥, Shashi Aithal*, Donald R. Wilson⊥

* HyPerComp Inc., 31255 Cedar Valley Dr., Suite 327 Westlake Village, CA 91362

⊥MAE Department, UT-Arlington, Arlington TX 76019-0018

Abstract:
This report is divided into three parts:

In the first part we present our ongoing work on the optimization of an MHD energy by-pass concept. Here we consider the optimization of the power generator and accelerator components individually, and are in the process of a simultaneous optimization of an integrated generator-combustor-accelerator concept in a 2-D sense. We have concentrated our efforts on developing an optimization scheme that couples a flow solver (perfect gas Euler and equilibrium gas N-S) with a Poisson solver for the electric field including Hall effects. The architecture/algorithm of the optimization scheme is such that geometric and/or physical parameters can be optimized for a given set of free-stream conditions and objective function. The objective function was MHD power extracted in the case of a MHD generator, and thrust in the case of an accelerator.

The second part of this report presents some ideas on how to extend this development and the associated real-gas MHD technology at HyPerComp Inc. into a potential Phase-II. We have developed a higher (4^{th} order and beyond,) order accurate solver for MHD developed under an AFRL contract. We consider possibilities involving the usage of this solver in accurate boundary layer calculations and plasma effects in shear layers as a potential Phase-II extension. The current study of energy bypass concepts may itself be extended into an extensive exploration of finite rate processes in such systems coupled with an efficient optimization routine based on adjoint methods.

A masters thesis supported in part by this contract on the optimization problem setup for hypersonic inlets to improve mass capture has been completed. Relevant portions of this thesis have been appended to this report in the third part.

Part-I

Optimization study of the MHD energy bypass engine concept

1.1 MHD with energy bypass – the associated optimization problem

At HyPerComp, we have in the past studied global flow control for accelerators and hypersonic inlets using MHD. Further, there are studies from the literature that provide analytical results in MHD power generator optimization. Test data to validate numerical models is available in plenty due to the interest in this subject in the 1960s and to some small extent, even in the present time. Due to the high confidence level in the prediction and optimization of MHD power generator/accelerator design, as well as some recent AFRL interest in energy bypass concepts (Refs [3,6]), we resolved to choose the following problem as a demonstration of Phase-I progress:

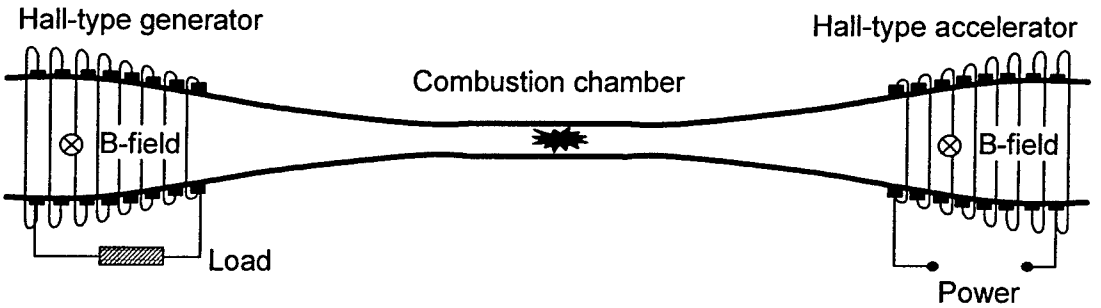

Figure-1: Energy bypass concept for hypersonics with an integrated MHD generator/accelerator

An integrated MHD power generator/accelerator system coupled through a combustion chamber where a fixed amount of heat is added to the system will be optimized to obtain the best geometric parameters. Applied magnetic field will be fixed, and a Hall-type system will be used to obtain best performance from the device. An equilibrium air Navier-Stokes solver will be coupled with a Poisson solver which will compute the electric field. Due to the need for fine segmentation in the electrodes to overcome the loss of efficiency due to the Hall effect, a special set of boundary conditions will be used at electrode walls. Electrical conductivity produced by seed substances as well as non-equilibrium e-beam ionization can be studied using our codes. However, we will restrict Phase-I work to include only equilibrium reacting air with alkali seed. The team from UT-Arlington will conclude their investigation on adjoint techniques initiated in the earlier progress report. Further, they will perform trial studies on hypersonic inlets with MHD wherein they will attempt to optimize the mass capture at off-design conditions using an applied magnetic field in the plane of the flow.

The success of Phase-I research will demonstrate the use of optimization techniques in the design and estimation of the potential performance of energy bypass devices being proposed for hypersonic flight. It will also produce a problem formulation which may be extended in Phase-II to study alternate "local" MHD flow control applications that are beyond the scope of phase-I study.

1.2 MHD power generator / accelerator

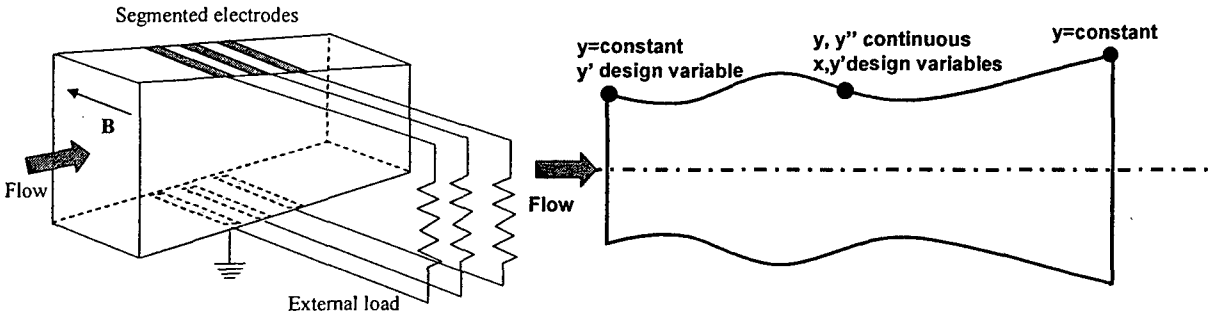

Figure 7: Schematic for MHD power generator optimization study

The theory of MHD power generators and that of flow accelerators is very similar in nature and is in a fairly mature stage, having been an active area of research since the 1960s (the ideas date back to Faraday!). Interest in optimizing their design came from worldwide efforts to build them and the conviction that their efficiency would be high compared to the-then available power producing methods due to the high temperatures of the working medium and the ability to dispense with expensive rotating machinery such as in turbines. Starting from the work of Neuringer [11], several analytical studies (1,15) have been performed to study the optimization problem. A recent study attempted to study the same problem (ref. [5]), quite characteristically unaware of the wealth of prior technical literature in the subject.

The recent development of advanced modeling ability in the area of MHD and plasma physics (e.g., Gaitonde [3] among others,) has enabled researchers to use CFD to assess the possibility of in-flight MHD power generation and flow acceleration, particularly for energy bypass concepts as discussed in refs [3,6]. We propose now, to use the studies of refs [3,6] as a baseline and perform a formal design optimization study, albeit 2-D in phase-I, to assess the sensitivity of its performance to various design parameters.

In this report, we merely present an overview of the physics and some sample results that validate the modeling of Hall-type power generators using MHD codes at HyPerComp.

1.2.1 Ohm's law relevant to Hall generators and accelerators

The appropriate form of Ohm's law relevant to MHD power generation or flow acceleration must include the Hall effect and may be then written as:

$$\vec{J} = \sigma(\vec{E} + \vec{V} \times \vec{B}) - \frac{\omega\tau}{B}(\vec{J} \times \vec{B})$$

The electric field (applied or induced,) must be divergence and curl-free and can be derived from a scalar potential. It is also at times customary to define a total electric field as the field observed by a particle traversing with the local velocity of the medium. These statements can be expressed mathematically as:

$$\vec{E} = -\vec{\nabla}\varphi, \; \vec{E}^* = \vec{E} + V \times B$$

We assume a two dimensional flow, in which velocity and electric field components only have x and y components. At each domain boundary or computational cell face, a normal vector and an accompanying tangent vector may be defined. We use the following notation for these vector quantities:

$$\vec{E}^* = (E_x^*, E_y^*), \quad V = (u, v), \quad \hat{n} = (n_x, n_y), \quad \hat{\tau} = (\tau_x, \tau_y) = (-n_y, n_x)$$

The final form of Ohm's law that is used in our computations is written as follows:

$$\boldsymbol{J} = \frac{\sigma}{1+\beta^2}\begin{bmatrix} \boldsymbol{E}_x^* - \beta \boldsymbol{E}_y^* \\ \boldsymbol{E}_y^* + \beta \boldsymbol{E}_x^* \end{bmatrix} = \frac{-\sigma}{1+\beta^2}\begin{bmatrix} (\varphi_x - \boldsymbol{B}v) - \beta(\varphi_y + \boldsymbol{B}u) \\ (\varphi_y + \boldsymbol{B}u) + \beta(\varphi_x - \boldsymbol{B}v) \end{bmatrix}$$

The divergence of the current density J derived above must identically vanish for an electrically neutral fluid. This results in a Poisson type equation for the electric potential which must be solved for an appropriate set of boundary conditions. We present some examples of such boundary conditions.

Electrode surface: An electrode is a constant potential surface. To this extent, one may clamp the potential of any one electrode in the domain to be the ground potential zero. However, any other electrodes present, must inherit a potential based on the exact layout of an internal/external circuit connecting these electrodes. In the case of an accelerator, a fixed potential difference may be applied across pairs of electrodes. While the potential of one electrode in a pair may be computed from an appropriate BC, the other is obtained by adding the voltage of the battery. In a generator, a load may be connected across a pair of electrodes and the potential difference may be inferred from the current circuited externally through the electrode pair.

Insulator: An insulating wall has zero current flowing normally into it. This can be used as a BC.

Infinitely segmented electrodes: The Hall effects diminishes the performance of MHD devices by producing current components normal to the principal direction of current production and diminishing the magnitude of the total current by a factor. Segmentation of the electrodes can somewhat alleviate this effect and improve performance. In a practical CFD code, modeling a very finely segmented set of electrodes is frequently infeasible due to the large demands on the mesh resolution. This issue can be resolved by the assumption of infinite segmentation, as discussed in Oliver and Mitchner [12]. The boundary condition to be used in such a case is that the current tangential to the region with infinitely segmented electrodes is zero. Further, these electrodes may be connected externally in order to reduce the transverse potential gradient in a "Linear Hall Generator". In such a situation, the potential of one row of electrodes is let to float subject to vanishing tangential current. The corresponding set on the opposite face are given a potential which is equal to it or determined from external loads connected between them.

1.2.2 Mathematical expressions for current BCs:

As mentioned earlier, we use two types of BCs on current related to its component normal or tangential to a wall. Using the notation from before, we may write these components as:

$$\begin{aligned} \boldsymbol{J}\cdot\hat{\boldsymbol{n}} &= \frac{-\sigma}{1+\beta^2}\left(\varphi_x \boldsymbol{n}_x - \boldsymbol{B}v\boldsymbol{n}_x - \beta\varphi_y \boldsymbol{n}_x - \beta\boldsymbol{B}u\boldsymbol{n}_x + \varphi_y \boldsymbol{n}_y + \boldsymbol{B}u\boldsymbol{n}_y + \beta\varphi_x \boldsymbol{n}_y - \beta\boldsymbol{B}v\boldsymbol{n}_y\right) \\ &= \frac{-\sigma}{1+\beta^2}\left(\varphi_x(\boldsymbol{n}_x + \beta\boldsymbol{n}_y) + \varphi_y(\boldsymbol{n}_y - \beta\boldsymbol{n}_x) - \boldsymbol{B}(V\cdot\hat{\tau}) - \beta\boldsymbol{B}(V\cdot\hat{\boldsymbol{n}})\right) \end{aligned}$$

$$\boldsymbol{J}\cdot\hat{\tau} = \frac{-\sigma}{1+\beta^2}\left(\varphi_x(\beta\boldsymbol{n}_x - \boldsymbol{n}_y) + \varphi_y(\boldsymbol{n}_x + \beta\boldsymbol{n}_y) + \boldsymbol{B}(V\cdot\hat{\boldsymbol{n}}) - \beta\boldsymbol{B}(V\cdot\hat{\tau})\right)$$

In the case when these components are to vanish, we can obtain convenient expressions for the gradient of the electric potential by rearranging terms, as below:

$$J\cdot\hat{\tau}=0\Rightarrow\varphi_y=\frac{\beta B(\vec{V}\cdot\hat{\tau})-B(\vec{V}\cdot\hat{n})-\varphi_x(\beta n_x-n_y)}{n_x+\beta n_y}$$

$$\varphi_x=\frac{-\varphi_y(\beta n_y+n_x)-B(\vec{V}\cdot\hat{n})+\beta B(\vec{V}\cdot\hat{\tau})}{\beta n_x-n_y}$$

$$J\cdot\hat{n}=0\Rightarrow\varphi_y=\frac{B(\vec{V}\cdot\hat{\tau})+\beta B(\vec{V}\cdot\hat{n})-\varphi_x(n_x+\beta n_y)}{n_y-\beta n_x}$$

$$\varphi_x=\frac{\varphi_y(\beta n_x-n_y)+B(\vec{V}\cdot\hat{\tau})+\beta B(\vec{V}\cdot\hat{n})}{n_x+\beta n_y}$$

The case of a linear Hall generator has been studied often in the past. Here, an infinite sequence of electrode pairs is short-circuited from outside. This makes the potential difference in the y-direction zero:

$$E_y=0$$

Current components can then be obtained by the somewhat simplified expressions:

$$J_x=\frac{\sigma}{1+\beta^2}(E_x+u\beta B),\quad J_y=\frac{\sigma}{1+\beta^2}(\beta E_x-uB)$$

Further simplification may result when studying the open-circuit condition wherein the current in the x-direction is zero in a one-dimensional sense. All field components can be derived analytically then.

1.2.3 Faraday-type MHD channel with Hall effect

We first present an MHD channel with a Hall parameter β = 1 and electrical conductivity = 1 (non-dimensional quantities). A Faraday type configuration is considered, where flat plate electrodes are used to cover a significant portion of the channel. These electrodes are held at a constant potential difference. Electric potential contours and current lines for such a flow are shown in Fig. [8] below.

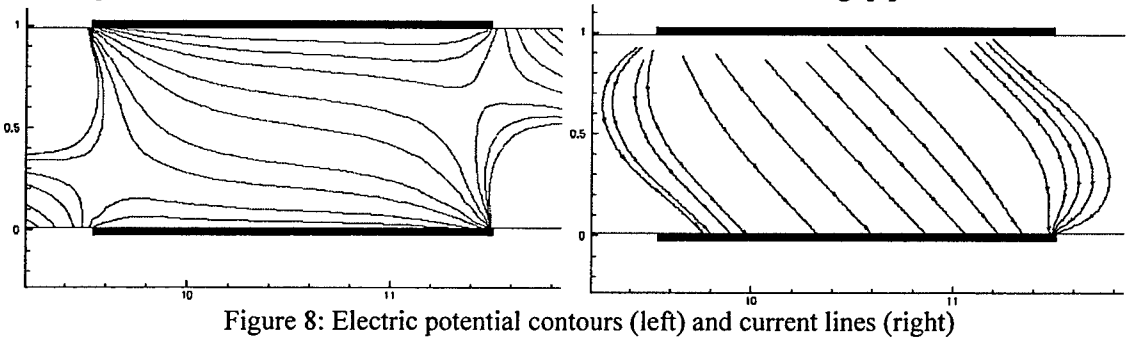

Figure 8: Electric potential contours (left) and current lines (right)

A characteristic feature of such a flow is the tendency of current lines to bunch upstream of the cathode and downstream of the anode in the presence of the Hall effect. The strong concentration of field gradients in these regions can cause damage to the electrodes, and is one of the perils of segmenting electrodes in MHD channels.

While the above describes the current features at the electrode-insulator boundary, the applied magnetic field has a very direct bearing on the induced current, as is shown in the following cases. The applied magnetic field is ramped up and held constant through most of the channel. All channel walls are assumed to be insulating here. The magnetic field is then evenly ramped down to zero. The regions of B-field

gradients show the presence of eddy currents, as seen in Fig. [9]. As the Hall parameter increases, these features develop asymmetries, and can eventually form very strong current components near the wall.

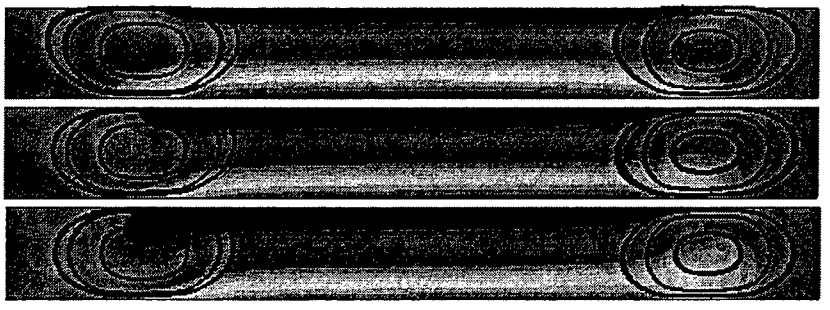

Figure 9: Current lines (above) and potential contours (below) for a channel flow with B-field gradients. Hall parameter is 0, 1 and 2 in the 3 images, in sequence.

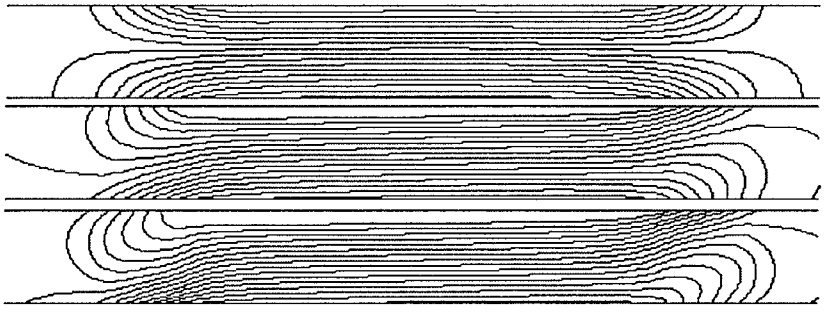

1.2.4 Infinitely segmented linear Hall generator

A very critical part of our approach to MHD/plasma flows is to model only verifiable physical phenomena for which there are adequate numerical models in the literature. The study of linear Hall generators is virtually a classical problem in MHD power generator studies and serves as an excellent test case in checking an MHD Poisson solver routine for boundary conditions and internal consistencies. We use the relations presented earlier for quasi-1D analysis to cross check the results from a 2-D calculation. The flow parameters are selected as follows:

$$u = 3.55, v = 0, \sigma = 1, \beta = 1, B_{max} = 1$$

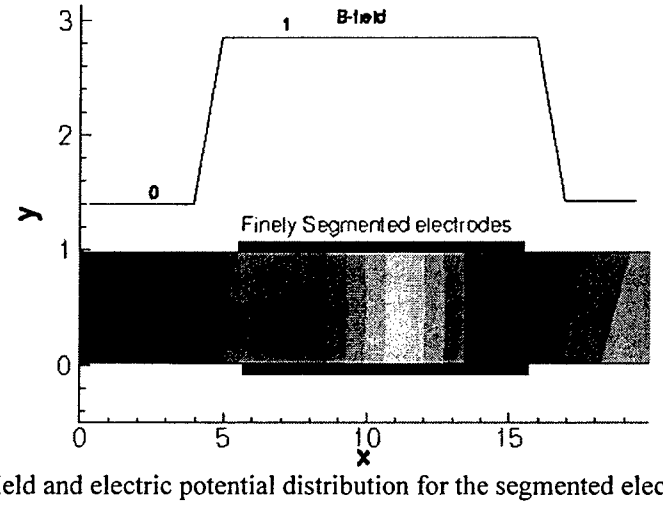

Figure 10: B-field and electric potential distribution for the segmented electrode generator

We present in Fig [11] the results from this calculation in the region of the Hall generator. Using the parameters listed earlier, and the relations in section [4.2] for a linear Hall generator, we must obtain a y-direction current density of $0.5(-uB + \beta E_x)$. The component Ex has been computed to be about -2.931. The value of uB is about -3.55. This gives a current density jy of about -3.24 which matches closely with the mean value shown in Fig. [11].

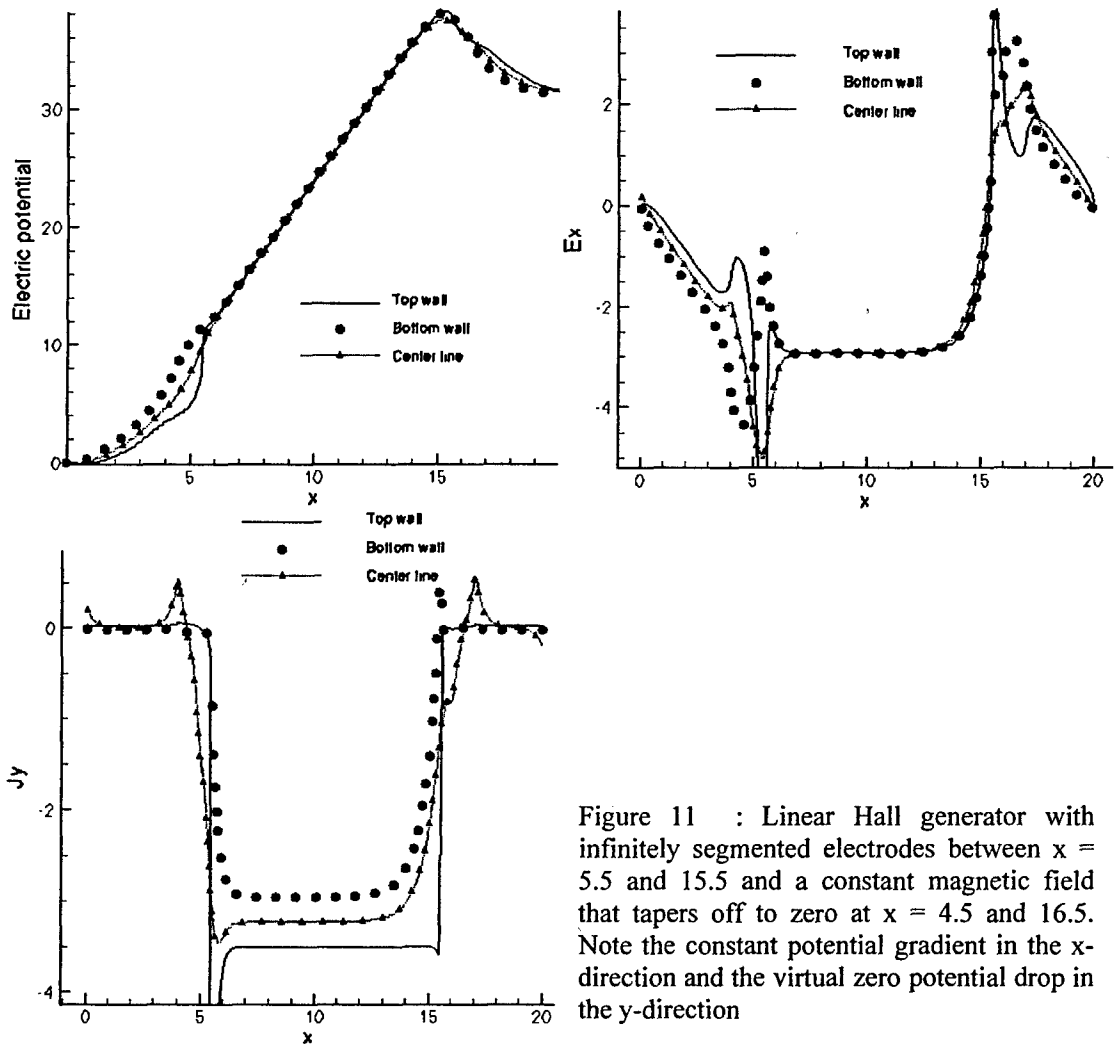

Figure 11 : Linear Hall generator with infinitely segmented electrodes between x = 5.5 and 15.5 and a constant magnetic field that tapers off to zero at x = 4.5 and 16.5. Note the constant potential gradient in the x-direction and the virtual zero potential drop in the y-direction

Further, it may be observed that the electric potential gradient in the y-direction is virtually zero, while a Hall voltage develops along the length of the channel. All these parameters are observed to be in good agreement with quasi-1D estimates, thus validating the MHD portion of this modeling effort.

1.3 Shape Optimization

In this study we concentrated on optimizing a single geometric parameter, in order to demonstrate the feasibility of our approach. This study was also intended to identify issues such as convergence criterion for the objective function, effect of grid-size on the search direction in the optimization routine and computing time for an optimization cycle. It was also aimed at identifying limits of physical parameters (electrical conductivity/interaction parameter) on the stability and convergence of the overall scheme. Optimization results shown here are for inviscid flows (Euler solutions). The results from these solutions would be good indicators to assess grid size and operating range (for design variables) for viscous flow simulations.

Figure 12 shows a generator/accelerator formed using a double cubic spline. The design parameters and their notations are explained in Table I. Variation of these design parameters can be used to optimize the shape of the accelerator/generator. In the results presented here, a single design parameter, (y'_o or y'_l) has been varied in the optimization process. The constraints on the design variables were that the slope be positive.

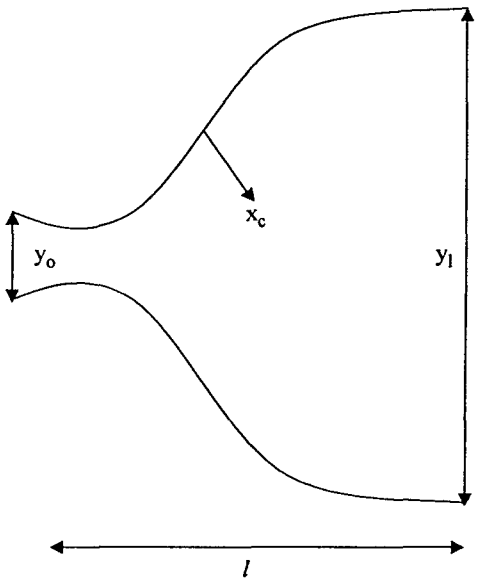

Table I

Parameter	Symbol
Inlet Diameter	y_o
Outlet Diameter	y_l
Location of end-points of spline	x_c
Slope at inlet	y'_o
Slope at outlet	y'_l
Slope at x_c	x'_o
Length of generator/accelerator	l

Figure 12: Schematic of geometry

Figure 13 shows the shape optimization for maximizing thrust when the design variable is y'_l. All other design variables shown in Table I were kept constant (see Table II). The initial value of y'_l is 10^0. The upper bound of y'_l was set at 40^0. The optimization process shows that increasing y'_l increases thrust.

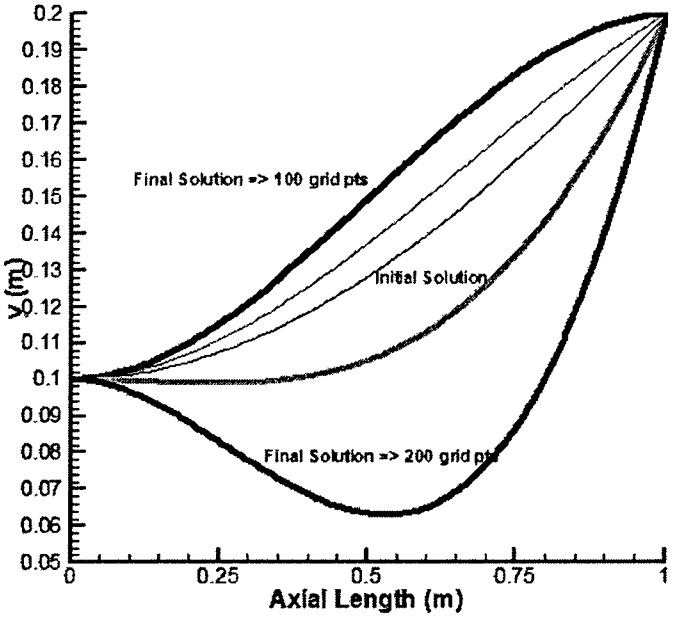

Figure 13: Shape optimization process, showing dependence of optimized shape on axial grids.

Table II. Parameters used in the shape optimization study

Parameter	**Symbol**
Inlet Diameter (y_o)	0.2 (m)
Outlet Diameter (y_l)	0.4 (m)
Location of end-points of spline (x_c)	0.0
Slope at inlet (y'_o)	0.0
Initial slope at outlet (y'_l)	10.0
Slope at x_c	0.0
Length of generator/accelerator (l)	1.0 (m)

An important consideration in shape optimization is determining the grid size so as not to influence the search direction in the optimization process. Table III shows the effect of axial grids on the optimization process. The results show converged values of the objective function (thrust) for $y_l' = 10$ degrees (red line in Figure 2). It is seen that when the number of axial grid points is below 200, the optimization search direction seeks a different local maxima. A particular geometry (corresponding to a given y_l') was considered to be converged (for all grids) if the variation in the objective function was less than 0.5% after an interval of 500 time-steps. Thus a fully converged objective function on a coarse grid might indicate a different optimized solution as compared to a fine grid. In this particular case, the coarser grid indicates that the thrust is maximum if the channel radius is monotonically increasing and the slope at the outlet is near zero. The fine grid solutions (200 X 60, 400 X 60 and 800 X 60) indicate however, that the thrust can be optimized if there is a constriction in the channel between the inlet and the outlet, thus implying that higher values of y_l', yield higher thrust. These considerations are important in deciding the minimum number of grid points to ensure unambiguous designs. Minimizing the number of grid points is of great importance in coupled MHD-viscous flow simulations as this is a computationally intensive process.

Table III: Variation of Thrust at the exit plane with axial grid size

Simulation #	Grid points	Thrust in KJ
1	100X 60	0.1945442
2	200 X 60	0.2582707
3	400 X 60	0.2924424
4	800 X 60	0.3096796

From Table III it is clear that the thrust varies less than 4% when the number of grid points in the axial direction is increased from 400 to 800. Hence this grid could be used to conduct further optimization studies. It was found that use of non-uniform grids in the radial direction did not change the value of thrust obtained using uniform grids.

1.3.1 Shape optimization of a MHD-accelerator (Euler solutions)

Based on the results in Table III, a 400X60 grid was used to study the shape optimization process with and without MHD for conditions shown in Table IV. These operating conditions (temperature/pressure and Mach number) are representative for operation of a MHD-bypass accelerator where seeding can be used to create the required ionization levels for MHD effects.

Table IV: Operating conditions for MHD accelerator

Inlet Pressure	0.1 atm
Inlet Density	1.38E-2 kg/m3
Inlet Temperature	2500 K
Inlet Mach Number	3
Electrical conductivity	1 mho/m
Max B-field	1 T
Hall Parameter	1
Applied Potential Difference	2000 V
Interaction parameter	$\cong 0.025$

Figure 3 shows the variation of thrust with y'_l with and without MHD effects. It is seen that the search direction with and without MHD is the same. Optimized thrust without MHD is less than that obtained with MHD. The electrical conductivity was kept constant at 1.0 mho/m in the flow field. The magnetic field (B) is as shown in Figure 14.

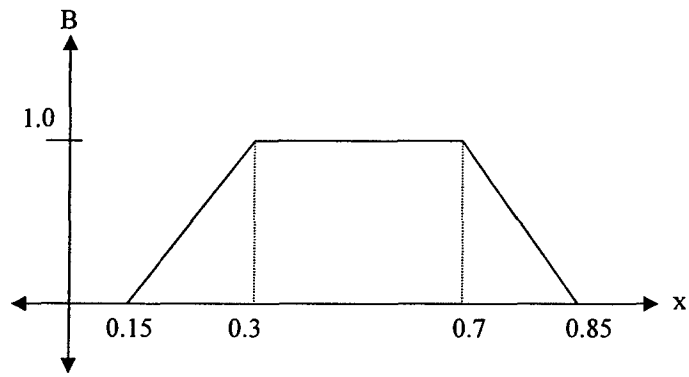

Figure 14: Variation of Magnetic field along axis of MHD accelerator

The maximum magnetic field is maintained in the middle of the accelerator in order to prevent MHD effects from creating instabilities at the inlet and outlet. The magnetic field is along the positive Z-axis (out of the plane of the paper). Figures 15 (a) and (b) show the Mach number contours with and without MHD effects. For a channel with an area-ratio of 2 and an inlet Mach number = 3.0, the isentropic value of the exit plane Mach number is 3.75. Figure 16 shows that the axial variation of the Mach number along the centerline of the accelerator. It is seen that the exit plane Mach number is about 3.5 without MHD and 3.8 with MHD. The increase in exit plane Mach number is small on account of the small value of the interaction parameter. Simulations are currently being run for higher values of interaction parameter.

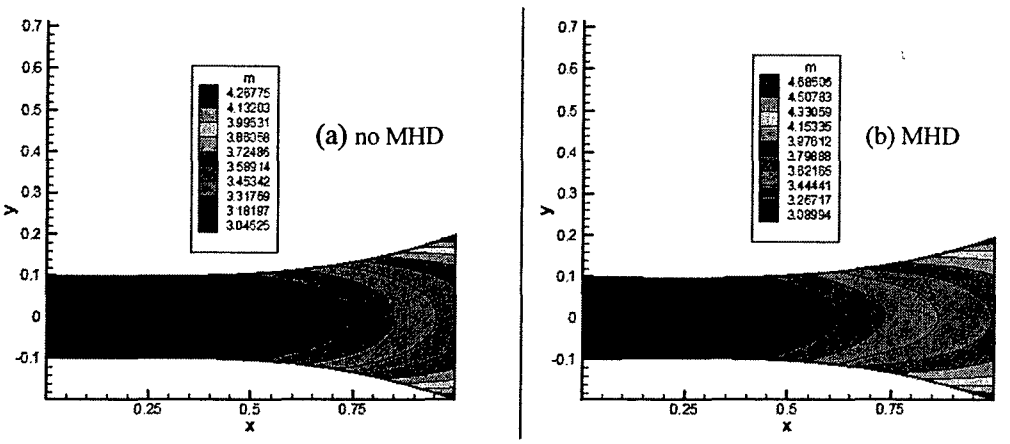

Figure 15 showing Mach number contours without and with MHD

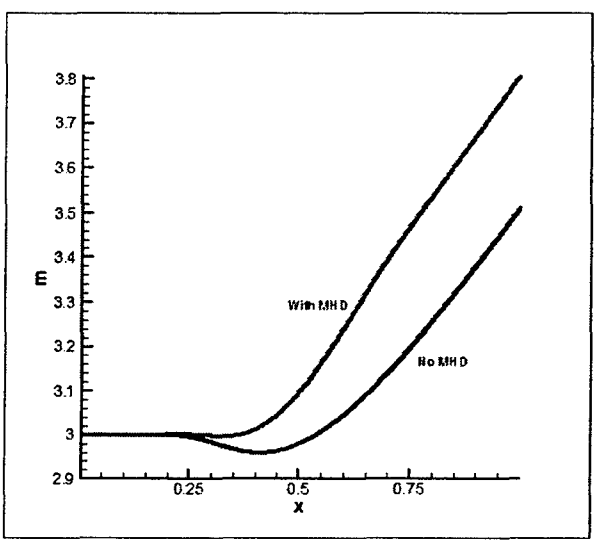

Figure 16: Axial variation of Mach number along the centerline.

Figure 17 shows contours of electric potential (φ) along with the current lines in the channel. The presence of the Hall effect is depicted in the field lines. It is seen that the current flows in the positive Y-direction thus producing a JXB force in the positive X-direction (along the flow) leading to flow acceleration.

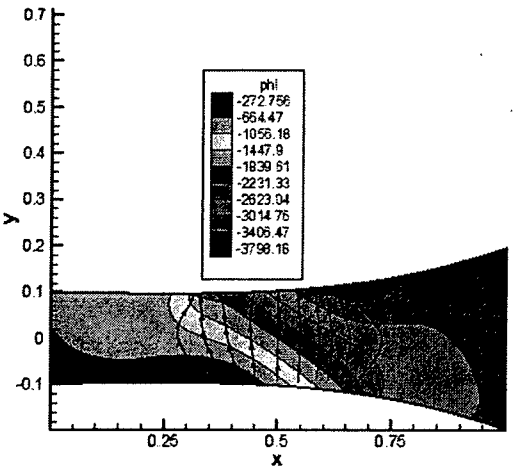

Figure 17: Contours of Electric Potential with current lines

1.3.2 Shape Optimization of an Infinitely segmented Hall generator generator (Euler Solutions)

Motivation for simulating a Hall generator:

In a typical hypersonic vehicle operating at Mach numbers below 10, air entering the MHD channel is at static pressures between 0.01 to 0.1 atm and temperatures around a few hundred Kelvin. The electrical conductivity of air under these conditions is very low (around 0.1 mho/m or less). Hence external on-board seeding or non-equilibrium methods are needed to generate and sustain electron number densities required to obtain electrical conductivities on the order of 10-30 mho/m. For a meaningful operation, power cost of
ionization should be much lower than the extracted electric power. This requirement suggests the use of strong magnetic fields (7-10 T) in order to generate an interaction parameter high enough for appreciable MHD effects. Low pressures and high magnetic fields lead to high Hall parameters, making it difficult to operate a MHD channel as a Faraday generator. A Faraday channel, allowing a longitudinal Hall current to flow would sharply reduce performance. The Hall current could be prevented by segmenting electrodes, but it this could still lead to engineering difficulties such as arcing and also deteriorate the performance of the Faraday channel.

Given these problems with a Faraday generator, it would be beneficial to use Hall configuration, where opposing pairs of segmented electrodes are short-circuited, and the longitudinal Hall current is collected. A Hall generator also seems like a natural choice, given the large Hall parameters characterizing a MHD-based hypersonic vehicle. Hall generators also promise to attenuate the electrode arcing problem on account of the large longitudinal current.

Results:

In practical MHD generators, keeping the surface area (volume) of a generator at a minimum is important from the standpoint of minimizing heat losses. A sample optimization problem based on this requirement, wherein the slope of the channel at the inlet was a design parameter was studied. Based on this angle, the length of the Hall generator (region where the top and bottom electrodes were shorted) was varied, so as to keep the total area of the generator constant. A higher slope at the inlet would just lead to a shorter axial length of the generator and vice-versa.

Figure 18 (a) shows the contours of electric field with current lines, whereas Figure 18 (b) shows the variation in inlet angle with optimization cycles to extract maximum power. The results indicate that a smaller inlet angle (and hence a longer MHD generator length) would yield maximum power while keeping the area fixed.

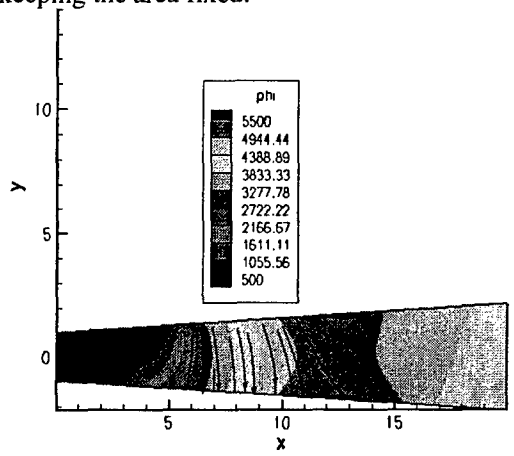

Figure 18(a). Electric field with current lines.

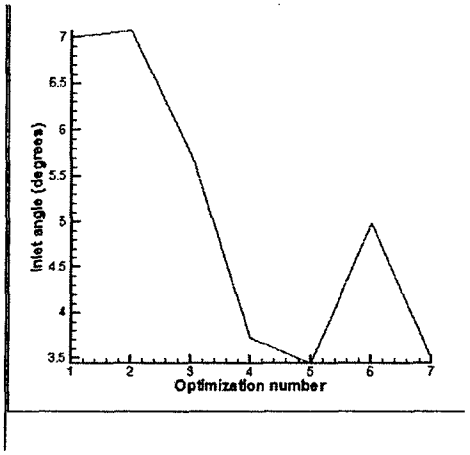

Figure 8(b). Iterative optimization of inlet angle

1.3.3 Viscous simulation of MHD Accelerator/generator:

The above results were obtained using an Euler solver for simulating the flow. These simulations are important in order to obtain a good estimate of the axial grids required and the upper and lower bounds for various design variables of interest to the problem. Viscous flow simulations of these high-speed flows require considerably longer time to converge, as it is necessary to resolve the thin boundary layers in these flows. A considerable amount of computing time can be saved if one were to conduct these N-S simulations in the neighborhood of the actual optimum solution.

As a part of our Phase I effort, we have developed a optimization scheme for viscous similar to the one with Euler solutions. This scheme is coupled with a CEA code which can determine the equilibrium chemical compositions for these MHD flow and compute realistic, spatially varying electrical conductivities and Hall parameters. The Poisson solver can thus simulate a realistic MHD generator/accelerator and thus be of immense use as a practical design tool.

Figure 19 shows the electric potential for an accelerator operating under the same flow conditions as mentioned above. The flow comprises of air seeded with about 0.02% of KOH at 2500K at the inlet, thus maintaining an electrical conductivity of about 10 mho/m.

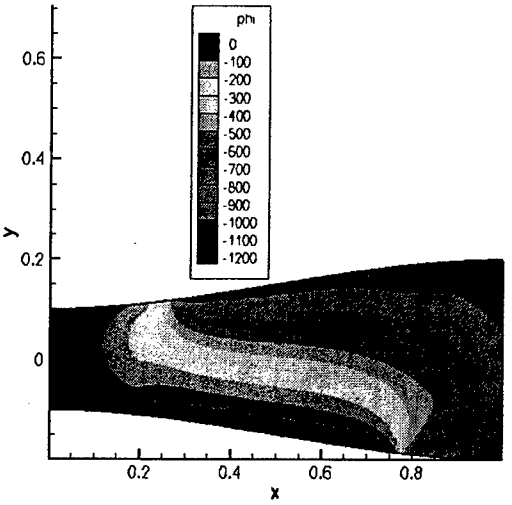

Figure 19: Contours of Electric field in N-S simulations.

1.3.4 Shape optimization of an MHD accelerator

We initiated a study of seeded air MHD accelerators partly because the conditions therein are close to equilibrium and an equilibrium property code such as CEA from NASA Lewis can be effectively used to model gas properties in such cases. Electrical conductivity is obtained from collisional cross section data and the local values of species concentration of the ionizing medium (in this case, air seeded with KOH). Air seeded in this manner develops a fair amount of conductivity at temperatures in the vicinity of 3000K.

We pose the following optimization problem:

Maximize the thrust produced by a nozzle:

$$T = \int_{exit} p_e - p_a + \rho u^2 \, ds$$

with a nozzle length of 1m, inlet width of 0.1 m and exit width of 0.5 m, by optimizing the contour of the nozzle surface defined by two con-joined segments shown in fig. [20]. The first is a circular arc segment of a radius of curvature 0.15 m, and the second is a cubic curve connected to the first at an angular location θ and having a y-coordinate of y1 at the exit plane. The design variables, therefore, are θ and y1.

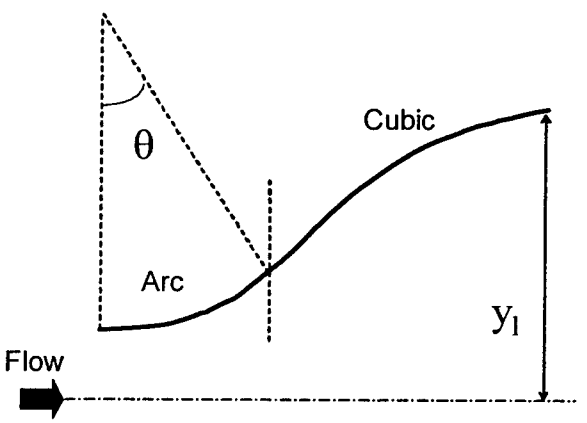

Figure 20 : Nozzle geometry for design optimization

A preliminary design study without the effect of MHD was made for such a nozzle geometry. Fig [21] shows a sample convergence history of the objective function and the arc angle as the optimization progresses. Nozzle inflow Mach number was selected to be 3 and an exit plane ambient pressure was selected to be the isentropic value for a "mean" area ratio of 5.

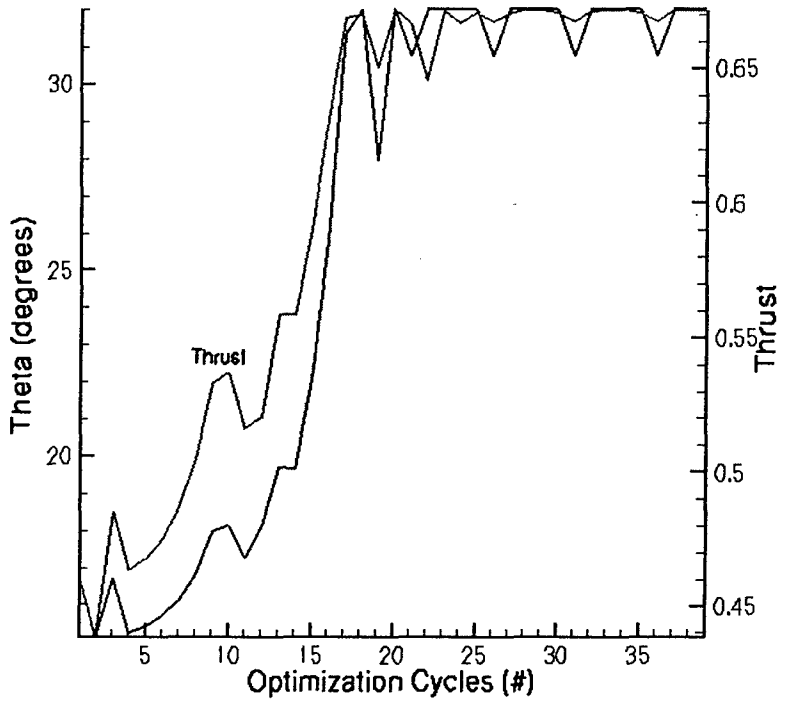

Figure 21: Nozzle thrust optimization with the arc-cubic geometry at inflow Mach number = 3

A central segment of such a nozzle was then powered by electrodes and a linear Hall-type generator was modeled. Using the "mean" design condition referred to above (based on isentropic flow), we attempt to obtain the load parameter K = Ey/uB of about 1.2. We select gas parameters such that the mean conductivity is about 2 mho/m. A magnetic field of 1 Tesla perpendicular to the plane of the flow was imposed in the powered region with linear taper on either side. The value of the applied electric field was 3600 V/m, perhaps corresponding to batteries of about 360 – 450 Volts connected across the channel. We present results from this design problem below.

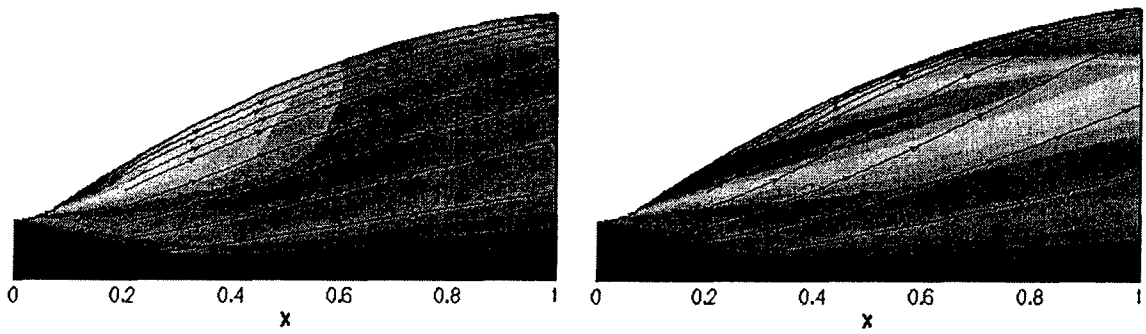

Figure 22: v-component of velocity with MHD (left) and without MHD (right)

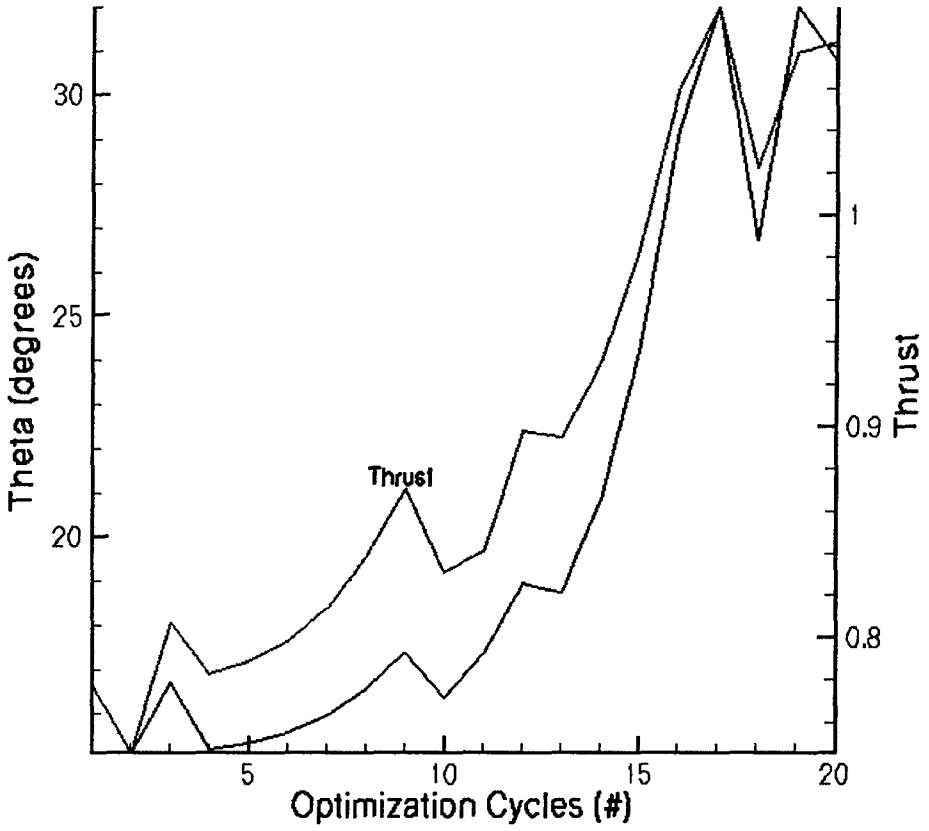

Figure 23: Optimization history showing the arc angle variation with thrust

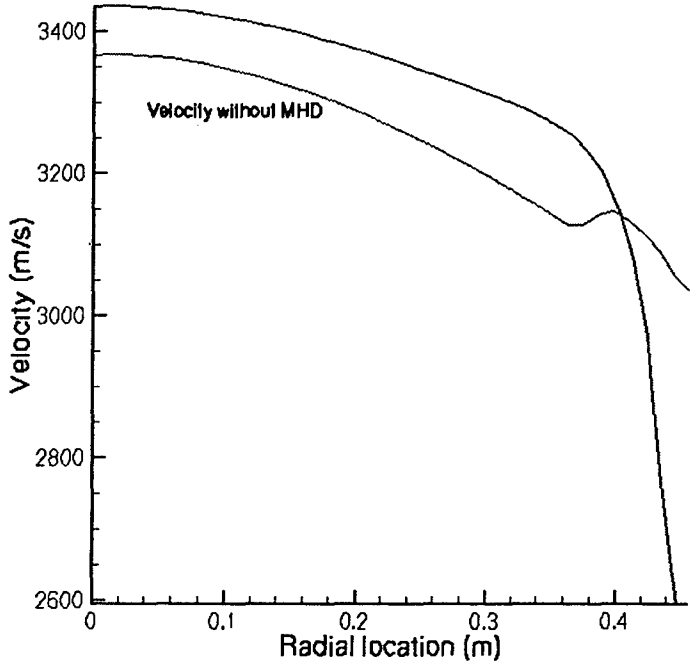

Figure 24: Exit plane velocity profile with and without MHD. Note the sharper drop in the velocity near the wall with MHD.

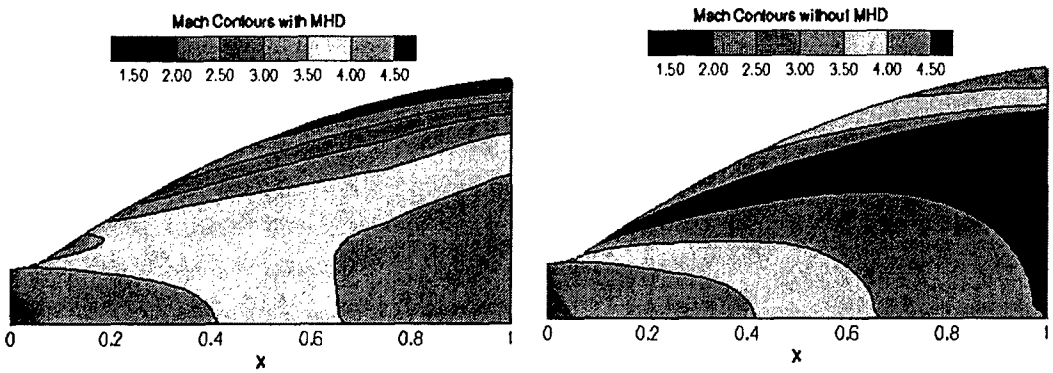

Figure 25: Mach number contours – note that for these conditions, exit Mach number in the MHD case is actually slightly lower than without MHD, while the velocity is actually higher.

1.4 An integrated MHD generator-accelerator model

We made a preliminary study of the coupled MHD generator-accelerator configuration. Two casese were studied, the first being a flat duct with specialized areas for power generation, combustion and flow acceleration. The second case was that of a piecewise linear geometry.

Case-I: Straight duct.

Lengths:
- Generator = 2.0 m
- Combustor = 2.4 m
- Accelerator = 3.3 m
- Total length = 7.7 m

Width = 0.5 m

MHD setup:
- Sigma (average) = 15.0
- Beta = 1.0
- Accelerator PD = 2000 V
- B-field = 1 T

Flow conditions:
- Inlet Mach No = 3.0
- Inlet Pressure = 0.1 atm
- Inlet Temp = 2500 K
- Inlet Velocity ~ 3000 m/s

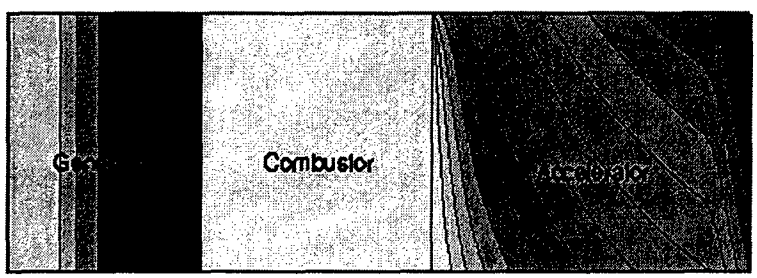

Figure 26: Contours of electric potential in the straight duct accelerator

The above conditions result in an interaction parameter of about 0.4. Figure above shows contours of electric potential in such a case. An effective power generated by the linear Hall generator was 0.12 MW, while the power used in the accelerator was 77 MW. Clearly, these are non-optimal and there is a very important role in parameter selection for even so simple a problem. If the system is to produce a net positive power, geometric as well as electrical parameters need to be selected correctly.

Case-II: Piecewise linearly varying duct.

Lengths:
- Generator = 2.0 m
- Combustor = 2.4 m
- Accelerator = 3.3 m
- Total length = 7.7 m

Widths:
- Inlet/Outlet = 0.6 m
- Combustor width = 0.3

MHD parameters:
- Sigma = 15.0
- Beta = 1.0
- Accelerator PD = 2000 V
- B-field = 1 T
- Interaction parameter ~0.4

Flow parameters:
- Inlet Mach No = 3.0
- Inlet Pressure = 0.1 atm
- Inlet Temp = 2500 K
- Inlet Velocity ~ 3000 m/s

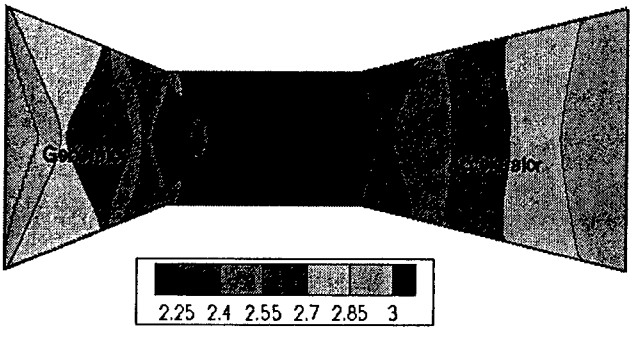

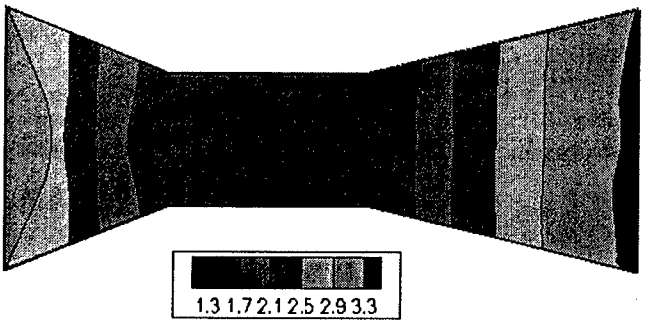

There is a vast potential for further investigations of this problem. Among the most important, from a systems perspective, would be the electrical coupling between the power generator and accelerator and how such a system may operate in a self-sufficient mode at a high efficiency for hypersonic/scramjet type applications. It may be noted that we have again used a seeded-equilibrium air type approach here for the sake of convenience. The introduction of non-equilibrium ionization would require the use of more complex numerical tools that are presently beyond the scope of this investigation, but would make an interesting and important research topic for a Phase-II project.

1.5 Summary of Results:

As a part of our Phase I research, we have concentrated on developing the tools and strategy to optimize MHD-based accelerator/generators. We have demonstrated the ability to simulate an MHD generator/accelerator and optimize their shape for a given design objective (maximizing power or thrust). We have developed the capability to include important physics (viscous effects, spatially varying properties such as electrical conductivities and Hall parameter) to simulate and optimize realistic operating conditions in a MHD by-pass concept.

Part-II

Plans for extension

Here, we present some possibilities for the extension of this work into a second phase. By way of applications, we wish to consider either the bypass engine concept studied earlier in the exploratory level in Phase-I, or the localized flow control concepts that are attractive.

2.1 Development of an optimal MHD-energy bypass propulsion system design

The optimal design of an MHD-energy bypass design for hypersonic vehicles presented here can be extended into Phase-II research. The design space will indeed be extremely complex, due to the vast diversity in time and length scales in the physics encountered. We present here a sampling of design variables that may potentially be chosen to model this problem.

The optimization problem itself can be one of the following:
1) Optimization of the total extracted power
2) Optimization of efficiency at a given power/length (minimization of losses)
3) Optimization of total cost subject to system requirements and engineering constraints

The given optimization problem can itself have many parameters which can be in one of the below mentioned categories.

1) Geometric factors
   - (i) length,
   - (ii) cross-sectional area,
   - (iii) number and location of electrodes,
   - (iv) electrode connections
   - (v) Distribution of external load for power extraction
   - (vi) Extent of the region for power extraction
   - (vii) Connection scheme between generator and accelerator
   - (viii) Efficiency of coupling between generator and accelerator

2) Physical factors
   - (i) strength of B-field
   - (ii) electrical conductivity (depends on seeding concentration, or beam current, beam energy, beam efficiency)

Figure below shows the 2-D schematic of a MHD bypass scheme consisting of an inlet, generator, combustor, and accelerator. The non-dimensional lengths, the reference length, typical magnetic fields and electrical conductivity are also shown in the figure.

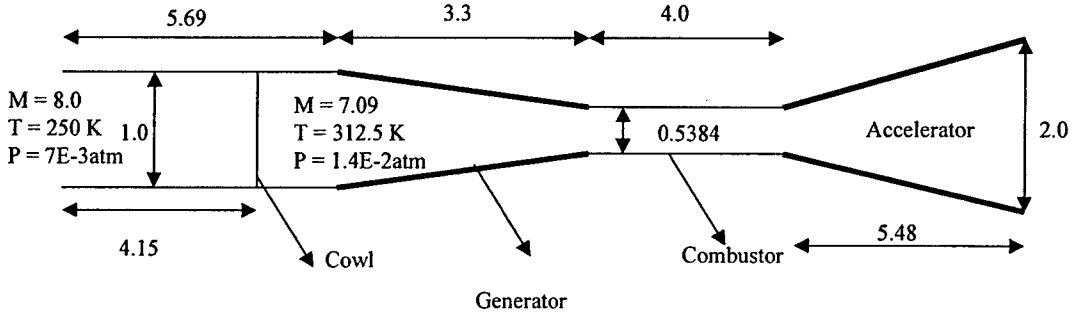

Sigma = 5 mho/m, B = 7 T
Lref = 0.6 m

The following figure shows an optimization problem comprising of a scheme where the design parameters are the coefficients of a double spline for both the generator and accelerator. The optimization problem could seek to maximize the extracted power in a generator and maximize thrust in the accelerator. The some possible design parameters for both the accelerator and generator are also shown in the figure.

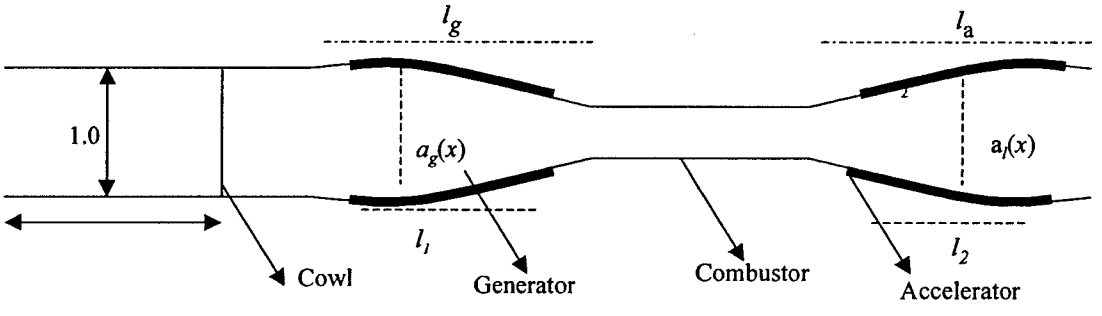

l_g = length of generator

l_1 = length of electrodes

$a_g(x)$ = cross-sectional area

$\{a_1,b_1,c_1,d_1,a_2,b_2,c_2,d_2\}_g$ = co-efficients of double spline for generator

l_a = length of accelerator

l_2 = length of electrodes

$a_l(x)$ = cross-sectional area

$\{a_1,b_1,c_1,d_1,a_2,b_2,c_2,d_2\}_a$ = co-efficients of double spline for accelerator

2.2 Shock-shock interaction and stagnation point heating

Avoidance of shock wave impingement on the lower cowl lip of hypersonic inlets is a critical problem in the design of hypersonic flight vehicles. Shock/shock interactions can result in an amplification of the usual stagnation point heat transfer rate by a factor of 30 or more. Edney[1] reduced shock/shock interactions to six types that depend on the orientation of the shock waves to the body. Only types III and IV involve a large value of the normalized heat transfer rate, q/q_0, where q_0 is the stagnation point rate without any interaction. Type III and IV interactions involve jets and shear layers that impinge on the surface of the body and result in extreme values of q/q_0.

One can, of course, design the inlet ramps so that shock waves do not impinge upon the lower cowl lip for the entire range of flight mach numbers, however, this leads to excessive spillage drag. Unfortunately, use of variable geometry to control shock wave position is often not feasible in hypersonic flight.

The typical optimization would involve control of shock position via MHD to minimize spillage drag (maximize capture ratio) over the entire flight Mach number range, without allowing the shocks to impinge on the cowl lip. This will be set up as constraints within the optimization procedure. The shock impingement will be forced to be at some clearance distance away from the cowl lip. A simple implementation of this strategy would be to increase the cowl length artificially and optimize for this configuration so as to maximize the mass capture, but forcing the overall configuration to cause intersection of the shocks at the tip of the artificially extended cowl.

2.3 MHD-Based Flow control

Turbulence, transition, drag reduction.

There is a growing resurgence of interest in the use of MHD to influence the lift and drag characteristics of airfoils and hydrofoils. The control of turbulent flows and transition using MHD is an almost classical MHD problem, which has reincarnated multiply in recent times. Tsinober has provided a review of flow control opportunities available here, and Henoch et al[8] have described an ongoing experimental program, which holds enormous promise, given its immediate relevance to seawater and possible extensions to plasma based devices in aeronautical engineering.

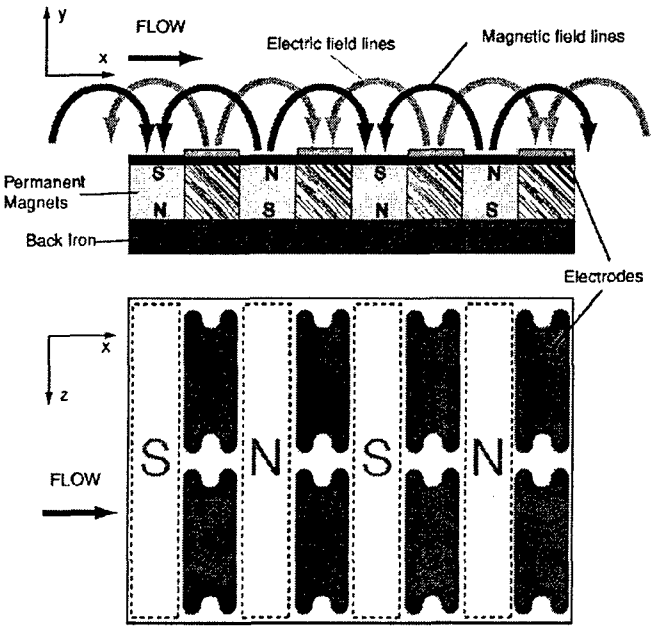

Figure 30: Lorentz force actuator to reduce turbulent skin friction, from Ref.[8] showing side and top views. Force acts in the spanwise direction. Electrodes are designed to reduce spanwise fringing fields.

2.4 Optimal MHD Adjoint Solution via the Hamilton-Jacobi-Bellman Equation

A generic adjoint based optimization procedure is outlined for an Objective Function, $J_c(U,\varphi,\theta)$ that depends on the flow variables U, electric field potential (and thereby on the current) φ, and the design parameters, θ.

$$J_c(U,\varphi,\theta) = \int_{\Omega} P(U,\varphi,\theta)d\Omega + \oint_{S} M(U,\varphi,\theta)ds \qquad (1)$$

For example, the problem could be the maximization of the mass weighted pressure loss for a hypersonic inlet where in $J_c(U,\varphi,\theta) = \frac{1}{\dot{m}P_\infty}\oint_S M(U,\varphi,\theta)ds$ and $M(U,\varphi,\theta) = \rho u \Delta y(P - P_\infty)$ or even the total mass capture at the inlet to avoid any spillage drag losses.

θ is the ramp angle and note, in this case along the stream-wise direction the change in the inlet area can be represented in terms of the ramp angle as, $\Delta y = (x - d)\tan\theta$, where d is the stream-wise location identifying the ramp vertex. The vector of state variables (characterizing the flow) are given by,

$$U = \begin{bmatrix} \rho \\ \rho u \\ \rho v \\ \rho E \end{bmatrix} \quad \text{and the Flux Vectors in Cartesian coordinates, } F = \begin{bmatrix} \rho \\ \rho u^2 + p \\ \rho uv \\ (\rho E + p)u \end{bmatrix} \qquad G = \begin{bmatrix} \rho \\ \rho uv \\ \rho v^2 + p \\ (\rho E + p)v \end{bmatrix} \qquad (2)$$

$$\boxed{\frac{\partial U}{\partial t} + R(U,\theta) = S(U,\varphi,\theta) \quad \Rightarrow \frac{\partial U}{\partial t} = f(U,\theta,t) \quad where, f(U,\theta,t) = -R(U,\theta,t) + S(U,\varphi,\theta,t)} \qquad (3)$$

The system of equations governing the flow (LHS) without the source term is purely Hyperbolic, while the source term by itself is computed as a solution to an Elliptic PDE.

We adopt an approach wherein, the flow solution is first computed, setting the source to zero and then utilizing the flow solution, the source term is computed, which is then substituted back into the flow equations for the solution in the presence of a non-zero source term and so on.

The objective function however depends on the flow variables, source term states and the design parameters.

For the Flux vectors described above, the Jacobians with respect to the flow variables are computed to be $\frac{\partial F}{\partial U}$ and $\frac{\partial G}{\partial U}$.

Hamilton-Jacobi Equation

For θ as the set of design variables, the flow fields physics is represented as $U(\theta)$ where U is assumed to be the solution of (3). Note that $R(U,\theta) = 0$, is the steady state PDE.

We assume that the computational domain and the primitive variables are the same and suppose that the cost function J_c is measured b (1).

This optimal cost problem is viewed in the sense of the optimization iteration number horizon, where a correspondence between the iteration number and the time horizon in conventional optimal control problems is hypothesized.

The justification is in the following observation:

Conventional Optimal Control Problem:

$$u(t) = -K(x,t)$$

is the feedback law that is sought to render some expected cost of the state deviations to be minimal. Here *u(t)* is the free variable (control) that is obtained as a function of the states of the dynamical system.

Flow Control Optimization Problem: The desired shape change is expressed as

$$\theta_{k+1} = \theta_k + \Lambda(U_k, \varphi_k),$$

Where, θ_k is vector of shape parameters at the kth iteration and $\Lambda(U_k, \varphi_k)$ is a function of the states of the dynamical system (flow solution).

Thus theoretically, for the infinite optimization horizon problem, we may cast this problem as one that seeks the optimal control strategy, over an infinite number of iterations.

Interestingly, these two problems viewed in the Discrete Optimization horizon and Discrete Time sense reduce to the solution of the Hamilton-Jacobi-Bellman equation that is summarized below.

For the system described in (3), with the steady solution, the performance index can be summarized as in (1)

The value function is then defined by, $V(U,\varphi,k) = \dfrac{\inf}{\theta(.)} \sum_{1}^{N} J_c(U,\varphi,\theta)$

The *dynamic programming principle* states that for every, $r \in [1 \quad N]$

$$V^*(U,\varphi,k) = \frac{\inf}{\theta(.)} \sum_{1}^{r} J_c(U,\varphi,\theta) + V(r, U(r), \varphi(r))$$

From the above we obtain,

$$V_{k+1}(U,\varphi) = V_k(U,\varphi) + H(\Psi, \nabla_\Psi V(U,\varphi)) \qquad \Psi = [U^T \quad \varphi]^T$$

also (4)

$$\frac{\partial V^*}{\partial t} = \frac{\partial V^*}{\partial \Psi} f(\Psi, \vartheta) + J_c(\Psi, \vartheta)$$

$$V_0(U,\varphi) = 0$$

The Hamiltonian H is given as $H(\Psi,\lambda) = \dfrac{\inf}{\vartheta(.)} \left\{ J_c(\Psi,\vartheta) + \lambda^T f(\Psi,\vartheta) \right\}$

The nonlinear first order PDE in the discrete form is the dynamic programming PDE or Hamilton-Jacobi-Bellman equation. Further, the Hamiltonian is concave in the variable λ (since it is the infimum of linear functions).

Viscosity Solutions

The terminology for the viscosity solution comes from the *vanishing viscosity method*, which finds solution for (4) as a limit of $V^{\varepsilon} \to V^{*}$ of solutions to

$$-\frac{\varepsilon}{2}\Delta V^{\varepsilon} + F(\Psi, V^{\varepsilon}, \frac{\partial V^{*}}{\partial \Psi}) = 0 \qquad (5)$$

The Laplacian term $\frac{\varepsilon}{2}\Delta V^{\varepsilon}$ is used to model fluid viscosity (for the numerical solution of the HJB alone).

A numerical scheme can be constructed that provides the optimal shape function as well as the Value function based on several existent solvers. Posing the optimization problem as an optimal control problem this way, eliminates the need to solve the numerical gradients. Further, in case of the Adjoint developments, the evaluation of the Adjoints is not trivial especially when the influence of shape functions is to be evaluated on a far-field flow variable. The above approach alleviates these difficulties at the expense of the iterative computational cost (multiple sub-problems). The relative computational burden should lie in between the numerical adjoint solution and the numerical gradient solutions.

As opposed to the traditional and adjoint methods, where the focus is on trying to compute the gradient of the cost function with respect to the shape parameters, the focus of the solution to the HJB equation is to construct an approximation to a sequence of shape-changes that will lead to the minimum cost.

References

[1] Carter, C., "The optimization of a magnetohydrodynamic generating duct," Brit. J. Appl. Phys., Vol. 17, pp. 863-871, 1966

[2] Corke, T.C., Post, M.L., "Overview of plasma flow control: Concepts, optimization and applications," AIAA 2005-0563, Presented at the 43rd AIAA Aerospace Sciences Mtg., Reno, NV, January 2005

[3] Gaitonde, D.V., "Simulation of local and global high-speed flow control with magnetic fields," AIAA 2005-0560, Presented at the 43rd AIAA Aerospace Sciences Mtg., Reno, NV, January 2005

[4] Korte, J.J., Auslender, A.H., "Optimization of contoured hypersonic scramjet inlets with a least-square parabolized Navier-Stokes procedure," Computing Systems in Engineering, Vol. 4, No. 1, pp. 13-26, 1993

[5] Kulkarni, N.V., Phan, M.Q., "Performance optimization of a magnetohydrodynamic generator at the scramjet inlet," AIAA 2002-5151, 2002

[6] Lindsey, M.F., McMullan, R.J., Gaitonde, D.V., "Development of a realistic 3-D scramjet flow path for MGD energy bypass," AIAA 2005-1178, Presented at the 43rd AIAA Aerospace Sciences Mtg., Reno, NV, January 2005

[7] McBride, B.J., and Gordon, S., "Computer program for calculation of complex chemical equilibrium compositions and applications – II: User manual and program description," NASA-RP-1311, June 1996

[8] Munipalli, R., Wadawadigi, G., Anderson, D.A., Wilson, D.R., "Application of optimization techniques in inlet design," AIAA 95-1824, 1995

[9] Munipalli R., Anderson, D.A., Wilson, D.R., "CFD evaluation of seeded and unseeded MHD accelerators," AIAA 2000-0215, 2000

[10] Nadarajah, S., Jameson, A., Alonso, J., "An adjoint method for the calculation of remote sensitivities in supersonic flow," AIAA 2002-0261, 2002

[11] Neuringer, J.L., "Optimal power generation from a moving plasma," J. Fluid Mech., Vol. 7, pg. 287-301, 1960

[12] Oliver, D.A., Mitchner, M., "Nonuniform electrical conductivity in MHD channels," AIAA Journal, Vol. 5, No. 8, 00. 1424-1432, 1967

[13] Opaits, D.F., Roupassov, D.V., Starikovskaia, S.M., Starikovskii, A.Yu., Zavialov, I.N., Saddhoughi, S.G., "Plasma control of boundary layer using low-temperature non-equilibrium plasma of gas discharge," AIAA 2005-1180

[14] Rosa, R., "Magnetohydrodynamic Energy Conversion," McGraw-Hill Book Company, 1968

[15] Shakhnov, I.I., Shcherbakov, V.T., "Optimization of MHD generators," Magnitnaya Gidrodinamika, Vol. 2, No. 4, pp. 49-54, 1966

[16] Shang, J.S., Surzhikov, S.T., Kimmel, R., Gaitonde, D.V., Menart, J., Hayes, J., "Plasma actuators for hypersonic flow control," AIAA 2005-0562, Presented at the 43rd AIAA Aerospace Sciences Mtg., Reno, NV, January 2005

Part-III

Extracts from the Masters thesis of Jennifer Goss at UT-Arlington

performed under the supervision of Prof. Kamesh Subbarao

SENSITIVITY ANALYSIS AND OPTIMIZATION OF
HYPERSONIC INLET PERFORMANCE SUBJECT
TO MAGNETOHYDRODYNAMIC EFFECTS

The members of the Committee approve the master's
thesis of Jennifer Dawn Goss

Kamesh Subbarao
Supervising Professor _____

Don Wilson _____

Seiichi Nomura _____

SENSITIVITY ANALYSIS AND OPTIMIZATION OF HYPERSONIC INLET PERFORMANCE SUBJECT TO MAGNETOHYDRODYNAMIC EFFECTS

by

JENNIFER DAWN GOSS

Presented to the Faculty of the Graduate School of
The University of Texas at Arlington in Partial Fulfillment
of the Requirements
for the Degree of

MASTER OF SCIENCE IN AEROSPACE ENGINEERING

THE UNIVERSITY OF TEXAS AT ARLINGTON

May 2005

ABSTRACT

SENSITIVITY ANALYSIS AND OPTIMIZATION OF
HYPERSONIC INLET PERFORMANCE SUBJECT
TO MAGNETOHYDRODYNAMIC EFFECTS

Publication No. _____

Jennifer Dawn Goss, MS

The University of Texas at Arlington, 2005

Supervising Professor: Kamesh Subbarao

This research considers the effects of magnetohydrodynamic source terms on the optimization of a scramjet inlet. A representative case is found by determining the optimal inlet configuration for the inviscid case assuming no MHD source. This is a simplified look into the optimization of the two ramp inlet say to a supersonic scramjet engine. The parameter being optimized is the mass weighted pressure loss at the throat of the inlet such that the pressure drop through the inlet is minimized. The optimal inlet configuration is then determined allowing for the presence of a charged flow through a magnetic field. This comparison will demonstrate the effects of the MHD source on the flow.

CHAPTER 3

OPTIMIZATION

Optimization is the process that finds the best or optimal solution for a given situation. There are three basic ingredients that make up an optimization problem:

1. An objective function $f(x)$ - That which we want to minimize or maximize.
2. A set of variables or unknowns $x = \{x_1, x_2, \ldots x_n\}$ - The parameters that will affect the value of the objective function.
3. A set of constraints - Limits set on the variables in any of the following forms:
   - equality $\rightarrow G_i(x) = 0, \qquad (i = 1, \ldots, m_e)$
   - inequality $\rightarrow G_i(x) \leq 0, \qquad (i = m_e + 1, \ldots, m)$
   - parametric bounds $\rightarrow x_{lower}, x_{upper}$

The optimization problem can then be stated mathematically as:

$$\min_{x \in \Re^n} f(x)$$

subject to

$$\begin{aligned} G_i(x) &= 0 \qquad (i = 1, \ldots, m_e) \\ G_i(x) &\leq 0 \qquad (i = m_e + 1, \ldots, m) \\ x_{lower} &\leq x \leq x_{upper} \end{aligned}$$

The type of optimization routine chosen to solve a particular problem is dependant on the size and characteristics of that problem. The size is influenced by the number of

design variables and constraints, and the characteristics describe the linear or nonlinear nature of the problem, this applies to the objective function as well as the constraints.

In our case the design variables are the two ramp angles, $x = \{\alpha_1, \alpha_2\}$. The objective function, $F_{obj}(x)$ we are trying to optimize is the mass weighted total pressure loss:

$$F_{obj} = \frac{\sum \rho_{i,j} u_{i,j} \Delta y_{i,j} (P_{i,j} - P_\infty)}{\dot{m} P_\infty} \tag{3.1}$$

where the i, j indices refer to the mesh points on the exit plane of the inlet and $P_{i,j}$ and P_∞ are the total pressures at the exit mesh points and at the entrance to the inlet respectively. And the constraints are the flow equations, solved by use of the flow solver as well as the condition that $\alpha_1 \leq \alpha_2$. We also set some upper and lower limits on the angles to ensure a well behaved result.

Our problem is therefore a constrained nonlinear multivariable problem in which we are going to implement a gradient based method. This type of method is generally the most efficient when the function to be minimized is continuous in it's first derivative. For functions that are highly nonlinear or have discontinuities, a search method that utilizes only function evaluations is more suitable. Where as higher order methods such as Newton's method, may be feasible for functions where the second order information is easily calculated.

3.1 BFGS Optimization

As mentioned, Newton's method is a higher order method that requires the calculation of Hessian, H at each step. This is a very computationally expensive procedure and can at times be very difficult. We there for look to a set of methods known as quasi-Newton or variable metric methods. Here an approximate Hessian matrix is built up gradually instead of calculating it at every single point. The build up of the Hessian is

done using gradient information from some or all of the previous iterations to formulate a quadratic model problem of the form:

$$\min_x \frac{1}{2}x^T Hx + c^T x + b$$

where the Hessian H is a positive definite symmetric matrix, c is a constant vector and b is a constant. The optimal solution for this problem occurs when the partial derivatives of f go to zero,

$$\nabla f(x^*) = Hx^* + c = 0$$

where the optimal solution x^* can be written as:

$$x^* = H^{-1}c$$

Quasi-Newton methods use the observed behavior of $f(x)$ and $\nabla f(x)$ to build up curvature information to make an approximation to H. The Broyden-Fletcher-Goldfarb-Shanno (BFGS) method is just one technique for the calculating the Hessian update. It is considered to be one of the most effective general purpose methods [26].

The BFGS optimization formula involves calculating a search direction in order to determine the descent direction that will locate the minimum.

$$d_k = {}^{-}H_k^{-1} \cdot \nabla f(x_k) \tag{3.2}$$

where $f(x)$ if the objective function and k denotes the iteration number. We start with an initial design vector x_0 and an approximate Hessian, H_0 which can be set to any symmetric positive definite matrix, *i.e.* identity matrix.

A one-dimentional search is performed in the search direction to determine the distance, α^* to be traversed in that direction. The design is then updated as:

$$x_{k+1} = x_k + \alpha^* d_k \tag{3.3}$$

The Hessian matrix is then updated as:

$$H_{k+1} = H_k + \frac{q_k q_k^T}{q_k^T s_k} - \frac{H_k^T s_k^T s_k H_k}{s_k^T H_k s_k} \tag{3.4}$$

where

$$\begin{aligned} s_k &= x_{k+1} - x_k \\ q_k &= \nabla f(x_{k+1}) - \nabla f(x_k) \end{aligned}$$

Gradient information is either supplied through analytically calculated gradients, or derived by partial derivatives using a numerical differentiation method via finite differences. This involves perturbing each of the design variables in turn and calculating the rate of change in the objective function.

The BFGS method implemented here is in the form of the 'fmincon' function in MATLAB® [1]. 'fmincon' is designed to find a minimum of a constrained nonlinear multivariable function [26]. It uses a Sequential Quadratic Programming (SQP) method where an estimate of the Hessian of the Lagrangian is updated at each iteration using the BFGS formula. The Lagrangian is the cost function augmented with the constraints:

$$L(x, \lambda) = F(x) - \lambda^T C(x)$$

[1]MATLAB/SIMULINK is the trademark of The MathWorks Inc; Natick, MA,USA

The function 'fmincon' was found to be very sensitive to the step size, as well as the scaling of the objective function itself. Several combinations of the above mentioned variables were tried in order to obtain the best results and it was found that a scaling of $ln(1 + Fobj^2)$ provided good convergence properties.

In order to ensure that we are still minimizing the correct function we state the following lemma:

LEMMA 1 (Modified Objective)

$$\min_x ln(1 + F_{obj}^2) = \min_x F_{obj}$$

Proof:

To find an extremum of a function we take the first derivative and set it equal to zero:

$$\frac{\partial}{\partial x} ln(1 + F_{obj}^2) = \frac{1}{1 + F_{obj}^2} 2F_{obj} \frac{\partial F_{obj}}{\partial x} = 0$$

This equation is only satisfied when $F_{obj} = 0$, which is a trivial solution, or when $\frac{\partial F_{obj}}{\partial x} = 0$, which is the same extremum as the original function, $\min_x F_{obj}$.

Now we wish to prove that this extremum is in fact the same extremum as that of the original function, we therefore take the second derivative and confirm that it is of the same sign:

$$\begin{aligned} \frac{\partial^2}{\partial x^2} ln(1 + F_{obj}^2) &= \frac{\partial}{\partial x} \left(\frac{2F_{obj}}{1 + F_{obj}^2} \right) \frac{\partial F_{obj}}{\partial x} + \left(\frac{2F_{obj}}{1 + F_{obj}^2} \right) \frac{\partial^2 F_{obj}}{\partial x^2} \\ &= \left(\frac{2F_{obj}}{1 + F_{obj}^2} \right) \frac{\partial^2 F_{obj}}{\partial x^2} \end{aligned}$$

since F_{obj} is a positive value, the result is simply a scaling of the second derivative of the original function, the sign is unchanged. This proves that extremum of modified objective function is of the same type as that of F_{obj}, therefore:

$$\min_x ln(1 + F_{obj}^2) = \min_x F_{obj}$$

3.2 Implementation

The implementation of this optimization routine is laid out in figure 3.1. As is shown in the flow chart the flow solution is calculated $n + 1$ times for each update of the Hessian, where n is the number of design parameters. The values of the objective function are stored from iteration to iteration for determination of the minimum and calculation of the gradients.

3.3 Results

The final optimized results of $\alpha_1 = 3.904\,\text{deg}$ and $\alpha_2 = 7.265\,\text{deg}$ are consistent with Korte's results of $\alpha_1 = 4.263$ and $\alpha_2 = 7.621$. The initial and final configurations are summarized in table 3.1. The initial condition was the shock cancelled case discussed earlier.

Fig. (3.2) shows the design history of the optimization routine at each iteration of the inside loop in Fig. (3.1). The outside loop iterations or number of times that the Hessian was updated, is equal to the total number of flow solver iterations divided by the number of design variables plus 1, $(\frac{iter}{(i+1)})$. From Fig. (3.1) we can tell that there were approximately 93 iteration of the flow solver and 2 design parameters, giving us approximately 31 update of the Hessian. The F_{obj} values plotted are scaled as per the scaling function mentioned earlier so as to improve the convergence properties. Fig. (3.3) is a plot of the Mach number contours for the final optimized configuration.

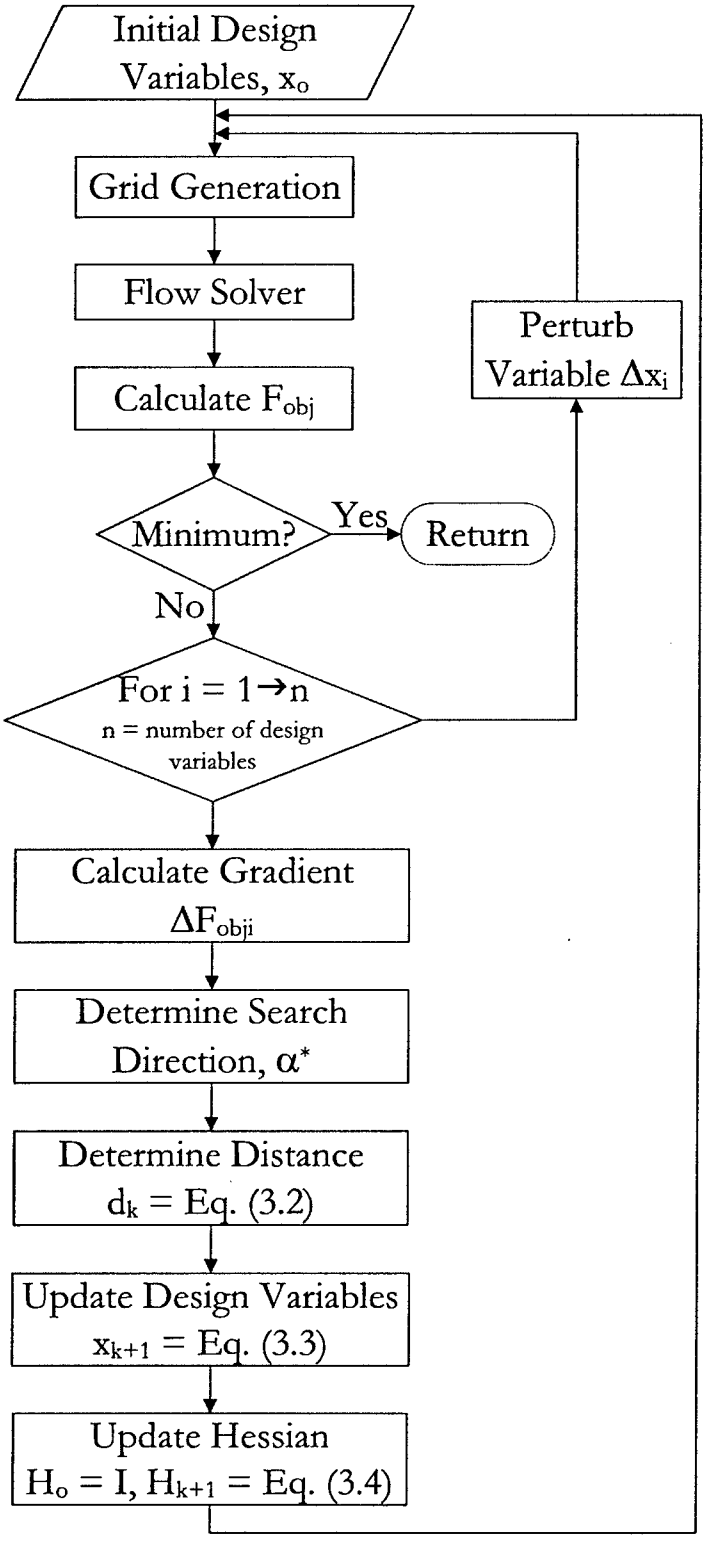

Figure 3.1 Flowchart of optimization routine.

Table 3.1 Summary of initial and final inlet conditions.

	α_1 (deg)	α_2 (deg)	F_{obj}
Initial condition	2.882	9.342	0.2445
Optimized value	3.904	7.265	0.1718

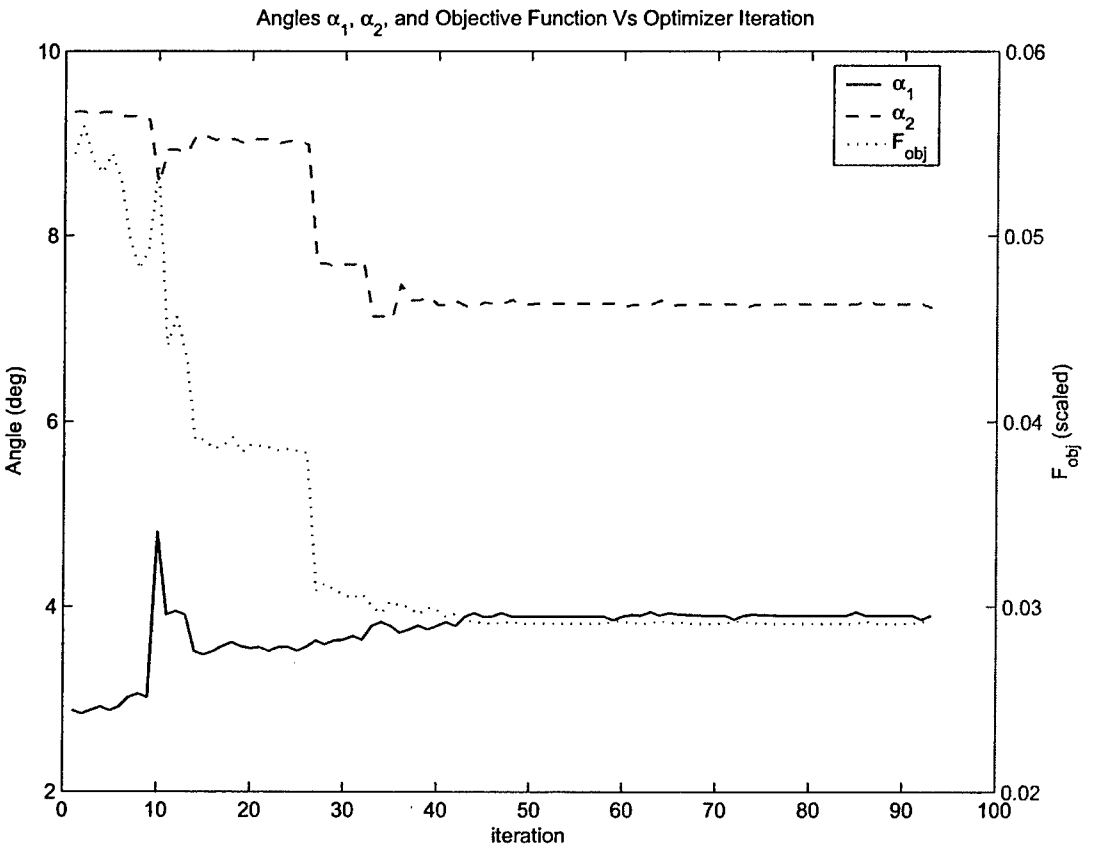

Figure 3.2 Optimization design history of ramp angles.

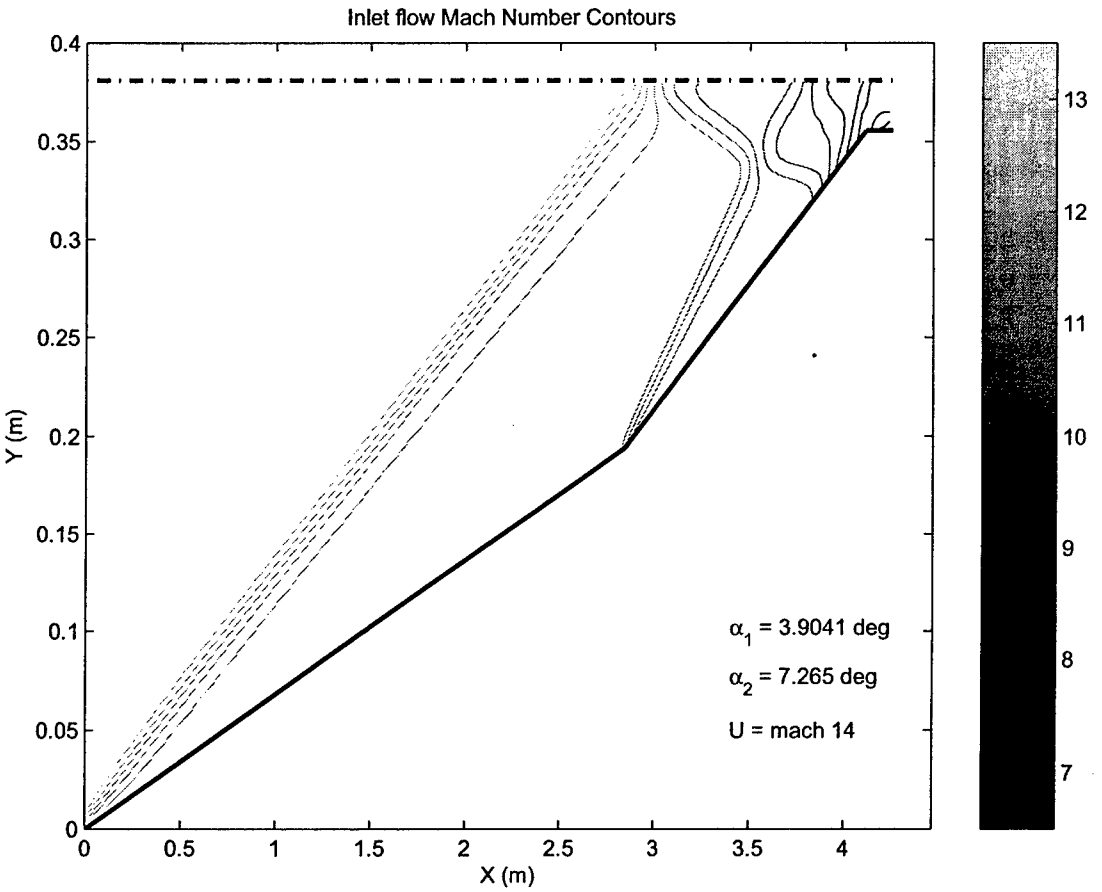

Figure 3.3 Final optimized inlet configuration Mach number contours.

CHAPTER 4

INVISCID EULER EQUATIONS WITH MHD SOURCE

4.1 MHD source term modelling

The effects of a charged flow through the inlet with an applied electromagnetic field can be modelled with the addition of appropriate electrodynamic terms [7]. Let us first consider a charged flow with conductivity, σ and velocity $\mathbf{V}$; if we apply a magnetic field, $\mathbf{B}$ to this flow the resultant current density is given as $\mathbf{J_B} = \sigma \mathbf{V} \times \mathbf{B}$. Whereas if an electric field, $\mathbf{E}$ is applied to the same flow the current density is given as $\mathbf{J_E} = \sigma \mathbf{E}$. The contributions to the electric field may be due to an applied electrostatic field $\mathbf{E_s}$, due to the mutual repulsion or attraction of electric charges, or an induced electric field, $\mathbf{E_i}$, due to the flow of charged particles through a magnetic field, such that $\mathbf{E} = \mathbf{E_s} + \mathbf{E_i}$. Thus the total current density in a flow with an applied electromagnetic field (neglecting Hall effect) is given by the generalized Ohm's law:

$$\mathbf{J} = \sigma(\mathbf{E_s} + \mathbf{E_i} + \mathbf{V} \times \mathbf{B}) \tag{4.1}$$

For the electrostatic field we know from Coulomb's law that $\mathbf{E_s}$ is irrotational and from Gauss's law that the divergence is fixed:

$$\begin{aligned} \nabla \times \mathbf{E_s} &= 0 \\ \nabla \cdot \mathbf{E_s} &= \frac{\rho_e}{\varepsilon_o} \end{aligned}$$

where ρ_e is the charge density and ε_o is the permittivity of free space. The induced electric field on the other hand has zero divergence and a finite curl governed by Faraday's law:

$$\begin{aligned} \nabla \cdot \mathbf{E_i} &= 0, \\ \nabla \times \mathbf{E_i} &= -\frac{\partial \mathbf{B}}{\partial t} \end{aligned}$$

We therefore have a total electric field $\mathbf{E} = \mathbf{E_s} + \mathbf{E_i}$, uniquely determined by:

$$\nabla \cdot \mathbf{E} = \frac{\rho_e}{\varepsilon_o}, \qquad \text{(Gauss's law)} \tag{4.2}$$

$$\nabla \times \mathbf{E} = -\frac{\partial \mathbf{B}}{\partial t}, \qquad \text{(Faraday's law)} \tag{4.3}$$

$$\text{and} \quad \mathbf{J} = \sigma(\mathbf{E} + \mathbf{V} \times \mathbf{B}) \qquad \text{(Generalized Ohm's law)} \tag{4.4}$$

MHD flows are characterized as having a very low (< 1) magnetic Reynolds number,R_m

$$R_m = \mu_o \sigma_g u L$$

where μ_o is the permeability of free space, σ_g is the gas conductivity, u is the gas velocity and L is a characteristic length.(High magnetic Reynolds numbers (> 1)are characteristic of fusion research and astrophysical phenomena). This tells us that the conductivity in MHD flows is very low, therefore the currents and hence the induced electric field is also very small. This allows us to assume $\mathbf{B}$ to be constant, therefore

$$\nabla \times \mathbf{E} = -\frac{\partial \mathbf{B}}{\partial t} \approx 0$$

As a consequence of the above we may introduce a scalar electrostatic potential φ such that $\mathbf{E} = {}^{-}\nabla\varphi$ and $\nabla^2\varphi = const.$ We can then replace the electric field term in the generalized Ohm's law, Eq. (4.4) with the electrostatic potential to get

$$\mathbf{J} = \sigma({}^{-}\nabla\varphi + \mathbf{V} \times \mathbf{B}) \tag{4.5}$$

Since $\nabla \cdot (\nabla \times \mathbf{E}) = 0$, Faraday's law, Eq. (4.3) implies that the magnetic field, $\mathbf{B}$ is solenoidal; $\nabla \cdot ({}^{-}\frac{\partial \mathbf{B}}{\partial t}) = 0$, therefore $\nabla \cdot \mathbf{B} = 0$.

The conservation of charge is given as,

$$\nabla \cdot \mathbf{J} = -\frac{\partial \rho_e}{\partial t}$$

this equation simply states that the rate at which the charge is decreasing in a small volume must equal the rate at which the charge flows out across the surface of that volume. For a stationary conductor ρ_e is zero, and when there is motion it turns out that ρ_e is very small and too low to produce any significant force, $\rho_e\mathbf{E}$ and therefore may be neglected. Based on these observations we conclude that

$$\nabla \cdot \mathbf{J} = 0$$

therefore, $\mathbf{J}$ is also solenoidal. Taking the divergence of Eq. (4.5). we can further simplify the generalized Ohm's law to get an expression for the electric potential

$$\nabla \cdot \mathbf{J} = 0 \qquad \Rightarrow \qquad \nabla \cdot \sigma(\nabla\varphi) = \nabla \cdot (\sigma\mathbf{V} \times \mathbf{B})$$

If we integrate both sides of this equation over a volume dV and use Gauss's theorem to convert the volume to a surface integral the equation becomes,

$$\begin{aligned} \int_V \nabla \cdot \sigma(\nabla\varphi) dV &= \int_V \nabla \cdot (\sigma \mathbf{V} \times \mathbf{B}) dV \\ \int_s \sigma \nabla\varphi ds &= \int_s \sigma \mathbf{V} \times \mathbf{B} ds \end{aligned}$$

We can now discretise this formula for use in our flow solver to calculate the MHD portion of the flow simply by summing up the contributions from each grid cell surface. For a given magnetic field and flow conductivity we can calculate the electric potential as follows:

$$\sum_{faces} \sigma_f \left(\frac{\varphi_N - \varphi_P}{\mathbf{d}} \right) \Delta\mathbf{s} = \sum_{faces} \sigma_f (\mathbf{V} \times \mathbf{B}) \Delta\mathbf{s}$$

$$\varphi_P = \frac{\sum_{faces} \sigma_f (\mathbf{V} \times \mathbf{B}) \Delta s - \sum_{faces} \sigma_f \frac{\varphi_N}{\mathbf{d}} \Delta\mathbf{s}}{\sum_{faces} \frac{\sigma_f}{\mathbf{d}} \Delta\mathbf{s}}$$

This allows us to then calculate the current density directly from Eq. (4.5), and it's impact on the flow equations is demonstrated in the following section.

4.2 Euler equations with MHD effects

As derived in chapter 2 the two-dimensional, nonlinear, Euler equations in conservative form for a compressible, inviscid flow are given as

$$\frac{\partial U}{\partial t} + \frac{\partial F}{\partial x} + \frac{\partial G}{\partial y} = S \tag{4.6}$$

With the application of a magnetic field to a charged flow the body forces and volumetric heating effects are no longer negligible. The body force term known as the Lorentz force are given by the vector $\mathbf{J} \times \mathbf{B}$, and volumetric heating known as Joule heating is given

as, $\frac{j^2}{\sigma}$. As seen earlier in the development of the Euler equations the contribution to the momentum equation is strictly due to the Lorentz forces where the contribution to the energy equation is the total rate of energy addition, $\mathbf{J} \cdot \mathbf{E} = \frac{j^2}{\sigma} + \mathbf{V} \cdot (j \times \mathbf{B})$ due to both volumetric heating and work done by the Lorentz forces.

In Eq. (4.6) U, F and G are as defined in the previous section and the source term, S is given as

$$S = \begin{bmatrix} 0 \\ (\mathbf{J} \times \mathbf{B})_x \\ (\mathbf{J} \times \mathbf{B})_y \\ (\mathbf{J} \cdot \mathbf{E}) \end{bmatrix}$$

The left hand side of Eq. (4.6) is unchanged from before, and as stated earlier this equation is hyperbolic for Mach numbers greater than one. The right hand side however is unconditionally elliptic for smooth variations of material properties, we therefore need to implement a Poisson solver to obtain the source terms.

4.2.1 Magnetic field perpendicular to the x-y plane

For a magnetic field applied to a conducting fluid, there is an induced electric field. Knowing this fact we must allow for the influence of the Hall effect in our equations, such that Ohm's law must be rewritten as follows

$$\mathbf{J} = \sigma(^{-}\nabla\varphi + \mathbf{V} \times \mathbf{B}) - \frac{\omega\tau}{\mathbf{B}}(\mathbf{J} \times \mathbf{B}) \tag{4.7}$$

the term $\omega\tau$ is called the Hall parameter where τ is the mean free time between collisions, and ω is the cyclotron frequency which for an electron with charge e and mass m_e, moving through a magnetic field of strength B, is equal to

$$\omega = \frac{eB}{m_e} \tag{4.8}$$

With the magnetic field implemented along the z-axis and utilizing the property of **J** being divergence free, we can convert Eq. (4.7) into a differential equation in terms of the electric potential. Let us first set the following notation:

$$\mathbf{V} = (u, v, 0), \qquad \mathbf{B} = (0, 0, B) \qquad \beta = \omega\tau, \qquad \alpha = \frac{\sigma}{1+\beta^2}$$

Then we can break down Eq. (4.7) into it's components:

$$\begin{bmatrix} J_x \\ J_y \\ J_z \end{bmatrix} = \begin{bmatrix} \sigma(^{-}\varphi_x + Bv) - \beta J_y \\ \sigma(^{-}\varphi_y - Bu) + \beta J_x \\ 0 \end{bmatrix}$$

Since we do not apply an external electrostatic field the only electric field present is due to the applied magnetic field and is restricted to the x-y plane thus the z-component of the electric potential, φ_z is zero. The current density components are therefore given by

$$\begin{bmatrix} J_x \\ J_y \end{bmatrix} = {}^{-}\alpha \begin{bmatrix} \varphi_x - \beta\varphi_y - Bv - \beta Bu \\ \varphi_y + \beta\varphi_x + Bu - \beta Bv \end{bmatrix}$$

and if we now enforce the divergence free condition on the current density, $\nabla \cdot \mathbf{J} = 0$

$$\frac{\partial}{\partial x}\left(\alpha\left(\frac{\partial\varphi}{\partial x} - \beta\frac{\partial\varphi}{\partial y} - vB - \beta uB\right)\right) + \frac{\partial}{\partial y}\left(\alpha\left(\frac{\partial\varphi}{\partial y} + \beta\frac{\partial\varphi}{\partial x} + uB - \beta vB\right)\right) = 0$$

grouping like terms

$$\frac{\partial}{\partial x}\left(\alpha\frac{\partial\varphi}{\partial x}-\alpha\beta\frac{\partial\varphi}{\partial y}\right)+\frac{\partial}{\partial y}\left(\alpha\frac{\partial\varphi}{\partial y}+\alpha\beta\frac{\partial\varphi}{\partial x}\right)=\frac{\partial}{\partial x}\alpha(vB+\beta uB)-\frac{\partial}{\partial y}\alpha(uB-\beta vB)$$

if we assume constant properties, α and β can be pulled out of the partial derivatives

$$\begin{aligned}\alpha\frac{\partial^2\varphi}{\partial x^2}-\alpha\beta\frac{\partial\varphi^2}{\partial x\partial y}+\alpha\frac{\partial^2\varphi}{\partial y^2}+\alpha\beta\frac{\partial\varphi^2}{\partial x\partial y} &= \frac{\partial}{\partial x}\alpha(vB+\beta uB)-\frac{\partial}{\partial y}\alpha(uB-\beta vB)\\ \nabla^2\varphi &= \frac{\partial}{\partial x}(vB+\beta uB)-\frac{\partial}{\partial y}(uB-\beta vB)\end{aligned}\quad(4.9)$$

Eq. (4.9) is the final form of the Poisson equation to be solved for this case.

4.2.2 Magnetic field in the x-y plane

If however, we implement a magnetic field in the $x-y$ plane and consider an ideally sectioned Faraday MHD generator such that the Hall effect is neutralized, the resultant current density is only in the z direction:

$$\mathbf{V}=(u,v,0),\qquad \mathbf{B}=(B_x,B_y,0),\qquad \mathbf{J}=(0,0,J)$$

$$\mathbf{J}=\sigma(^{-}\nabla\varphi+\mathbf{V}\times\mathbf{B})$$

$$\begin{bmatrix}J_x\\J_y\\J_z\end{bmatrix}=\sigma\begin{bmatrix}0\\0\\uB_y-vB_x-\varphi_z\end{bmatrix}$$

For this research we are setting φ_z to zero which corresponds to a short circuit of the electric field.

The source terms are then trivially found as follows without the need for a poisson solver:

$$S = \begin{bmatrix} 0 \\ \sigma \mathbf{B_y}(v\mathbf{B_x} - u\mathbf{B_y}) \\ \sigma \mathbf{B_x}(u\mathbf{B_y} - v\mathbf{B_x}) \\ \mathbf{J} \cdot \mathbf{E} \end{bmatrix}$$

4.3 Results

4.3.1 Magnetic field perpendicular to the x-y plane

To simulate an ionized flow we set the conductivity in a small pillbox area in the center of the inlet where the flow would most likely become ionized, to some chosen value, and the conductivity outside the box is set to $1e^{-}6$. For this case we oriented the magnetic field along the z-axis or out of the page with a uniform magnetic field strength of 1.0 tesla. As you can see in Fig. (4.1) the currents are indeed generated but only in the zone of simulated ionization, this is expected since the conductivity is negligible outside that zone. We used a full inlet in this case due to the non-symmetric nature of the problem. Fig. (4.2) demonstrates the effects that this current flow has on the Mach contours, the flow decelerates earlier and the pressure recovery at the inlet is decreased from the non-MHD case.

4.3.2 Magnetic field in the x-y plane

For a magnetic field implemented in the x-y plane there are no currents to be seen since they are generated perpendicular to the x-y plane. We ran a number of simulations with varying conductivity and magnetic field angle and these results are shown in Fig. (4.3) for two different magnetic field strengths.

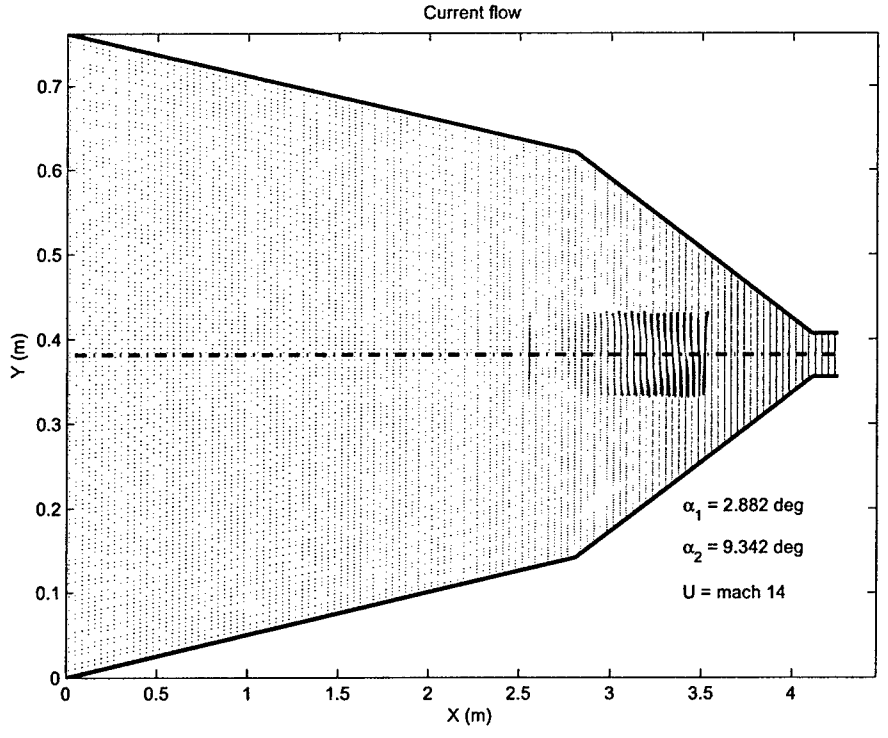

(a) Full inlet

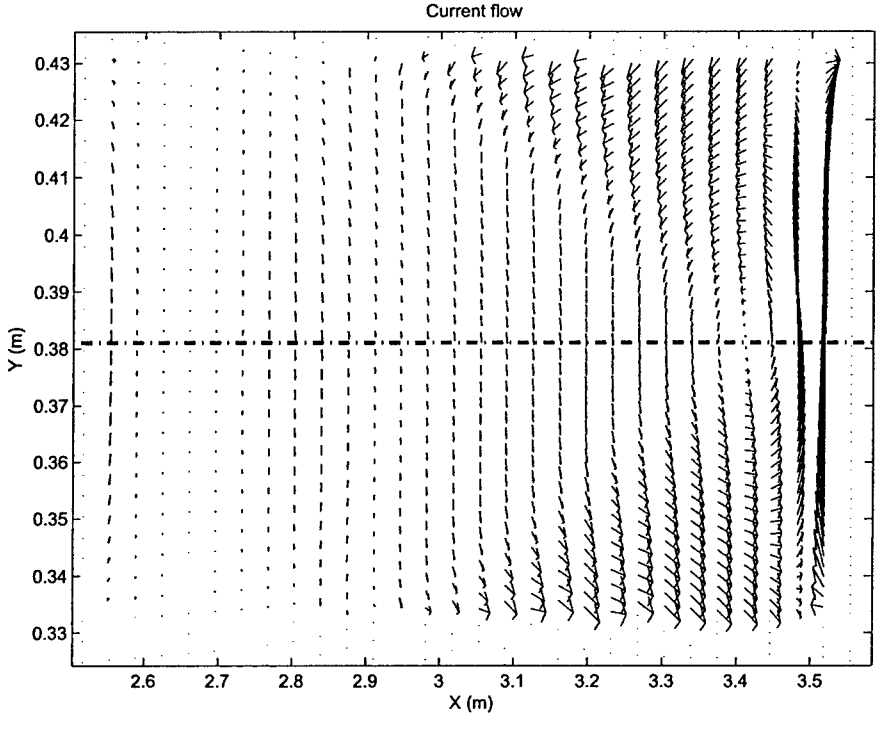

(b) Zoom in of pill box area

Figure 4.1 Inlet with current flow for a pillbox shaped conducting region. (b) is a closer look at the ionization zone which can be seen in the center of (a). σ inside the box is 50 mho/m.

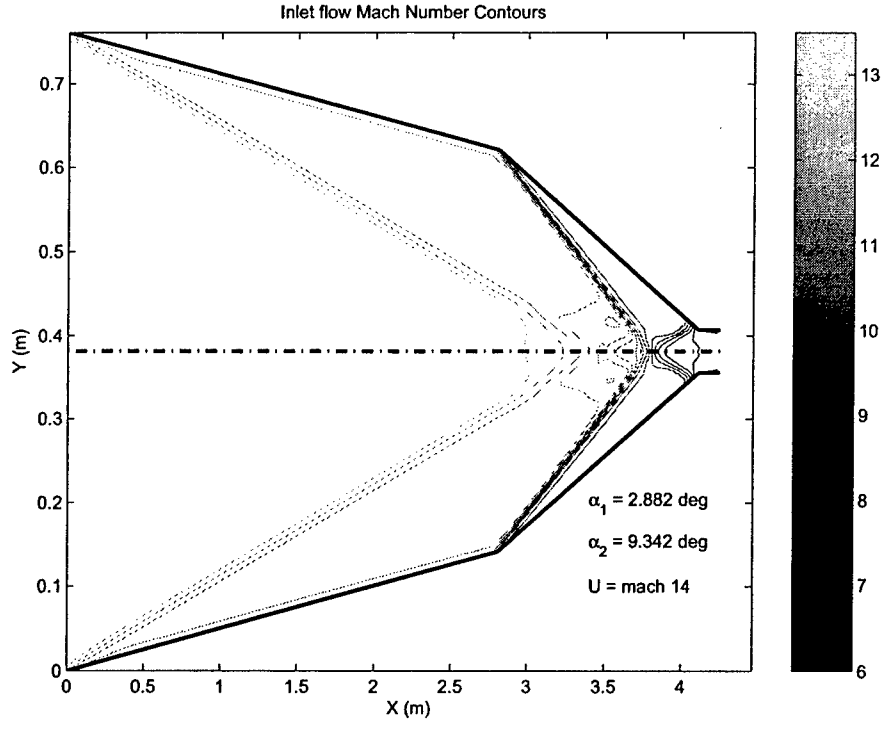

(a) Inside the box $\sigma = 10$ mho/m

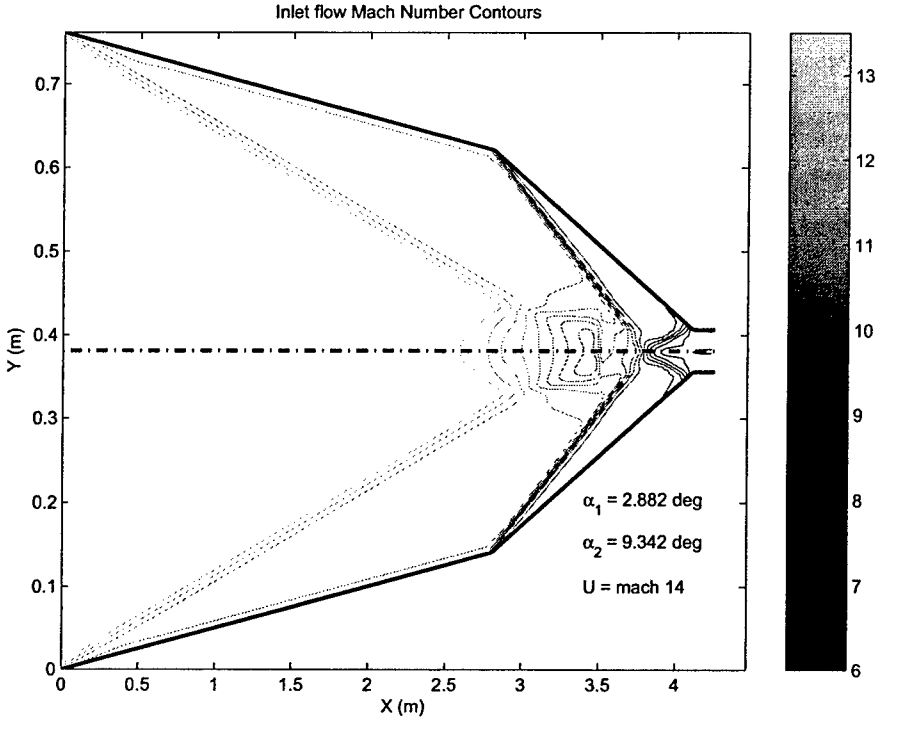

(b) Inside the box $\sigma = 50$ mho/m

Figure 4.2 Inlet Mach number contour plots for a pillbox shaped conducting region. Two values for the conductivity are shown, in (a) $\sigma = 10$ mho/m, (b) $\sigma = 50$ mho/m.

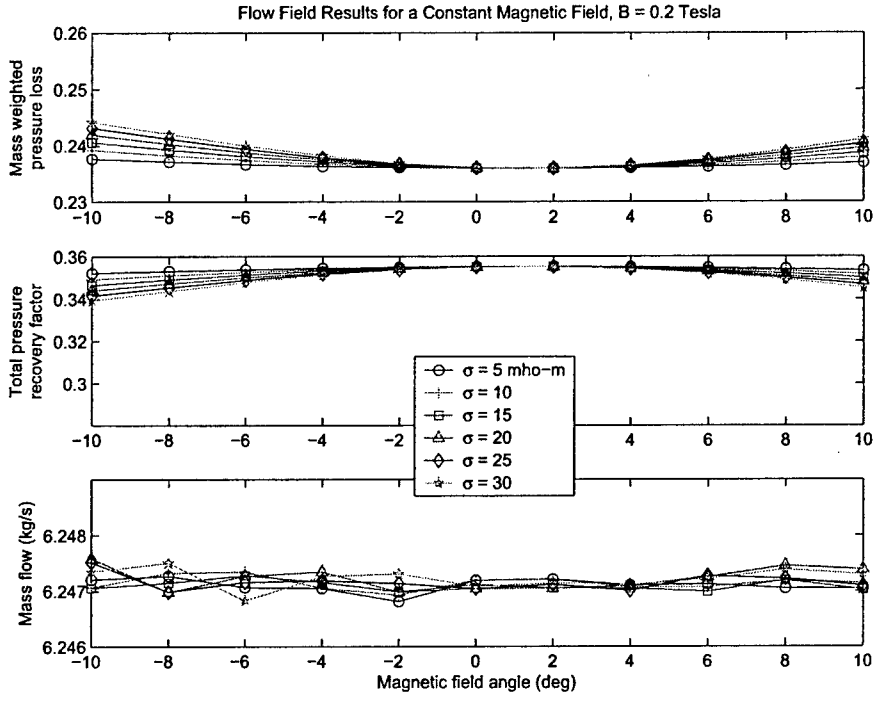

(a) Constant magnetic field B = 0.2 tesla

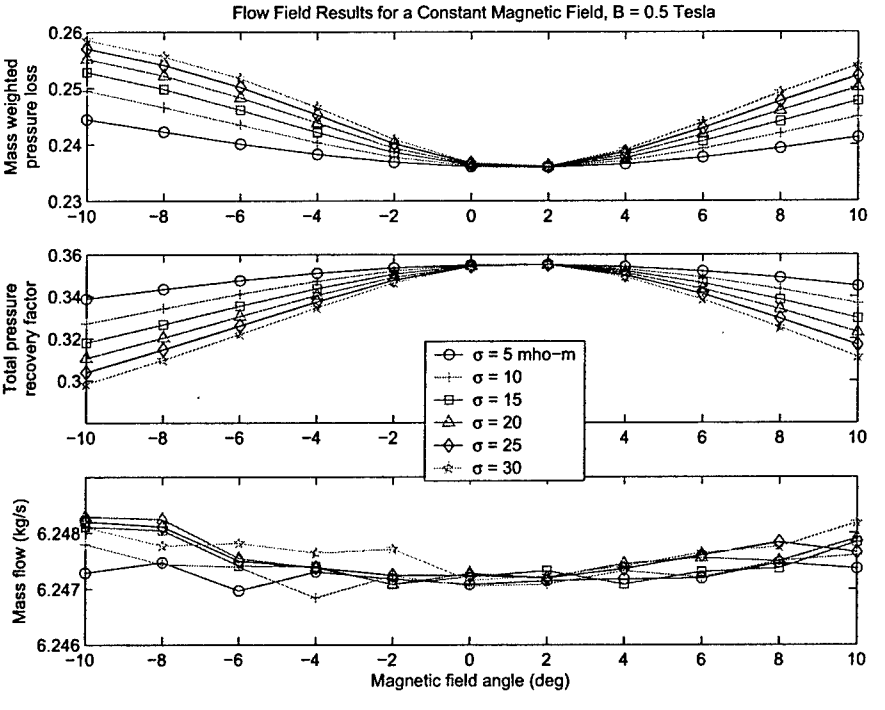

(b) Constant magnetic field B = 0.5 tesla

Figure 4.3 Mass weighted pressure loss, total pressure recovery and mass flow for a constant magnetic field with varying field angle and varying conductivity. The magnetic field strengths are (a) 0.2 tesla and (b) 0.5 tesla.

As can be seen in Fig. (4.3) the application of a magnetic field to the charged flow always results in a decrease in the pressure recovery (or an increase in the pressure loss). This is consistent with the theory in that we are not adding any energy to the flow and the resultant joule heating is only a detriment to the pressure recovery. We therefore adjust the problem to consider a cowl style inlet where we try to optimize the mass capture. The optimal situation for the cowl configuration can be seen in Fig. (4.4).

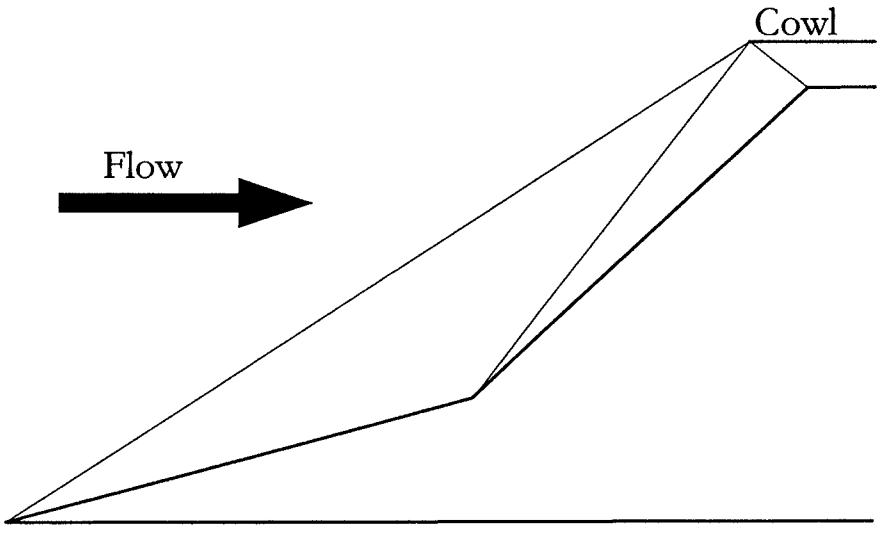

Figure 4.4 Optimal cowl configuration with shocks converging on the cowl lip.

To determine our optimal configuration we ran the optimizer with a mass capture objective function given as:

$$F_{obj} = \sum \rho_{i,j} u_{i,j} \Delta y_{i,j} \tag{4.10}$$

The results of which are shown in Fig. (4.5) where $\alpha_1 = 2.2$ deg, $\alpha_2 = 8.9$ deg and the mass capture equal to 6.1965 kg/s.

During off nominal flight conditions where the flow Mach number is less than the design value, the shocks will move ahead of the cowl lip and some of the compressed air

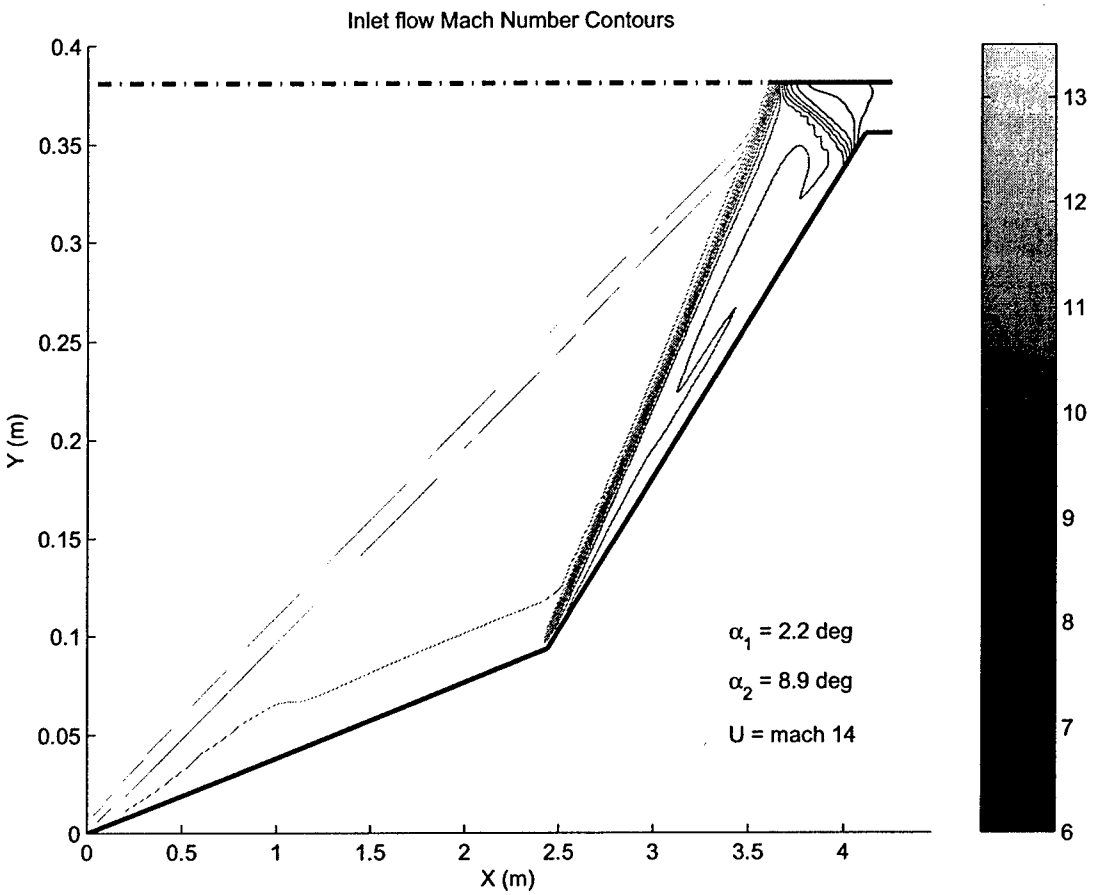

Figure 4.5 Mach contours of optimized cowl inlet.

will escape the inlet resulting in 'spillage' and a decrease in the mass capture. In flight conditions where the flow Mach number is greater then the design value, the shocks move into the inlet causing multiple reflected shocks, loss of total pressure, possible boundary layer separation and engine unstart [4]. Fig. (4.6) demonstrates these conditions.

To simulate a less than design Mach number flow we adjust the ramp angles to $\alpha_1 = 3.0$ deg and $\alpha_2 = 9.0$ deg which results in a mass capture of 5.8757 kg/s. See Fig. (4.7) for the Mach contours in this case.

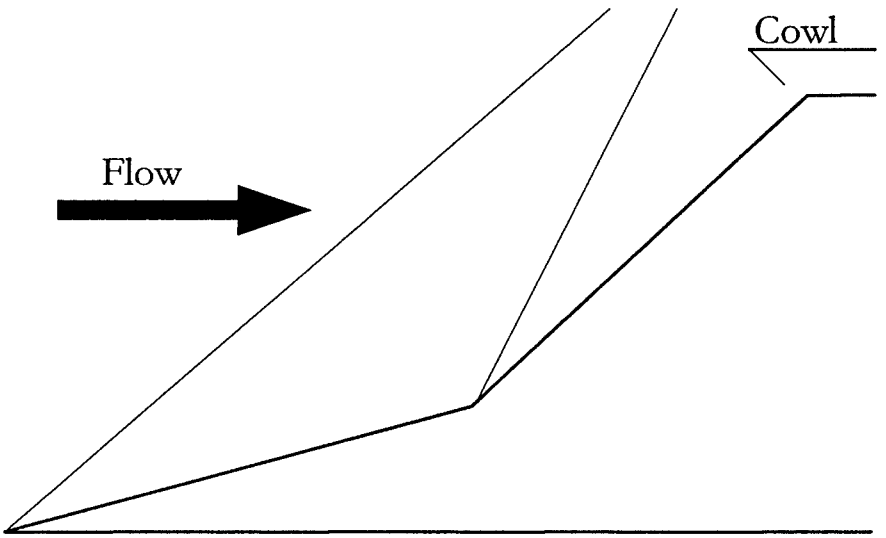

(a) Mach number less than design

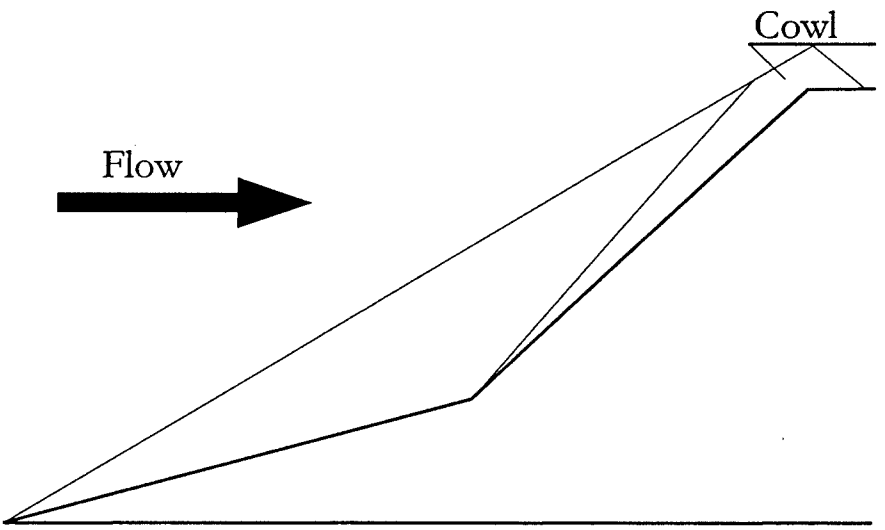

(b) Mach number greater than design

Figure 4.6 Off-nominal cowl configurations (a) shows a less than design Mach number, (b) shows a greater than design Mach number.

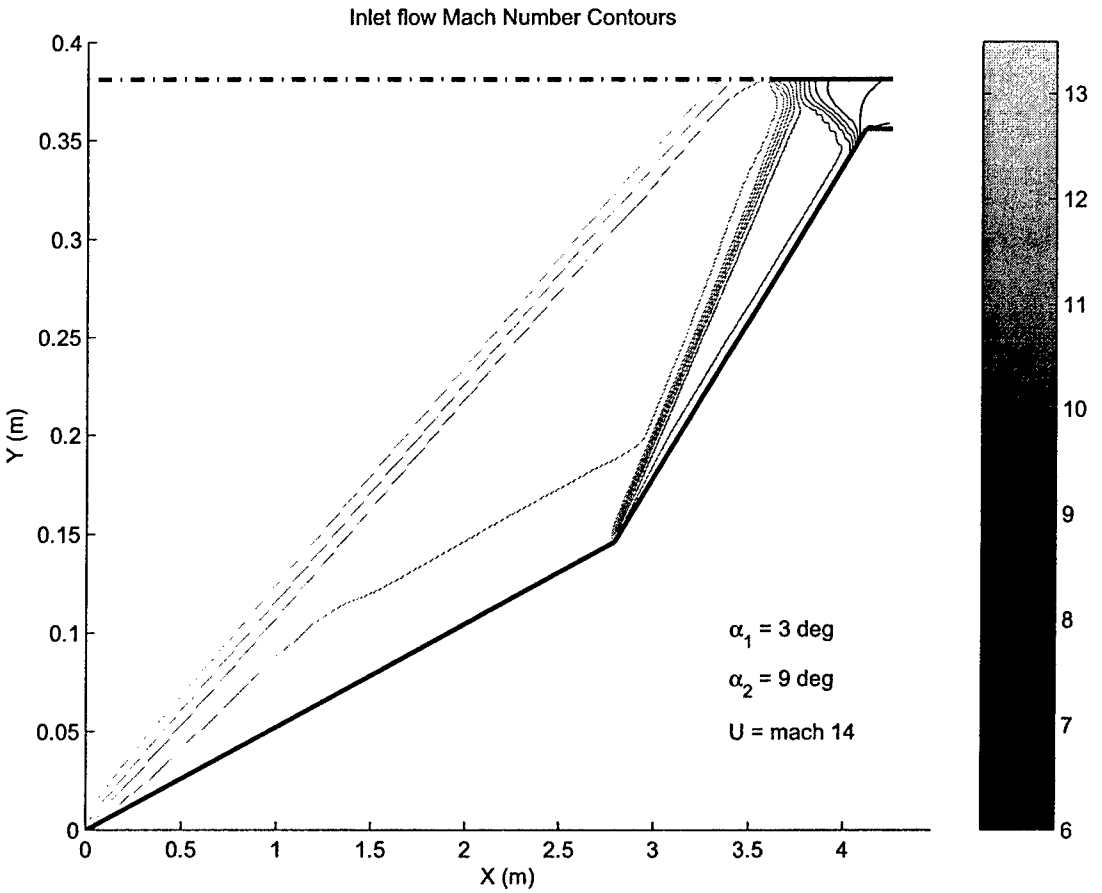

Figure 4.7 Mach contours for off nominal cowl inlet.

We now investigate the ability of an applied magnetic field to direct the flow back to the optimal mass capture configuration. Two different scenarios are considered; one is a moving e-beam type ionization method [3] such that the magnetic field and ionization region are movable and coincident, the second is a moving magnetic field but stationary ionized region [4]. Fig. (4.8) demonstrates each scenario. In the case of the e-beam ionization the ionized region is enclosed by within lines that are parallel to the magnetic field lines: $y_0 + (x - x_0 - \Delta x)\tan(\alpha) \leq y(x) \leq y_0 + (x - x_0 + \Delta x)\tan(\alpha)$, the line $y(x) \leq$

radius of inlet, and the body. The parameters x_0, y_0 and Δx determine the position and width of the ionized region.

Figs. (4.9) through (4.12) show the results of this study. It is clear from these results that the larger the magnetic field strength and the larger the conductivity the greater the influence on the flow. It is interesting to note that the stationary ionized zone has a much greater ability to manipulate the flow than the coincident ionized region. For the largest values of $\mathbf{B}$ and σ (line corresponding to $\mathbf{B} = 0.5$ in Fig. (4.12)), we can see that the mass capture is indeed approaching that of the optimal situation.

With the results from this broad parametric study we decided to set up the problem in the optimization routine and compare the results. This time we set the objective function as the mass capture Eq. (4.10), and the design variable was the magnetic field/electron beam angle alone. Aware of the sensitivities in the optimization routine we decided to try several different initial conditions to see how well the results converged. We decided on initial conditions of the implementation angle, θ_{Bi} above and below the approximate optimal values given by the parametric study. Tables (4.1) and (4.2) summarize the results.

Table 4.1 Table of optimized magnetic field angle for coincident ionized zone.

	θ_{Bi} below optimal	θ_{Bi} above optimal
Initial condition (deg)	100	170
Optimized value (deg)	141	165

Table 4.2 Table of optimized magnetic field angle for stationary ionized zone.

	θ_{Bi} below optimal	θ_{Bi} above optimal
Initial condition (deg)	80	140
Optimized value (deg)	108	111

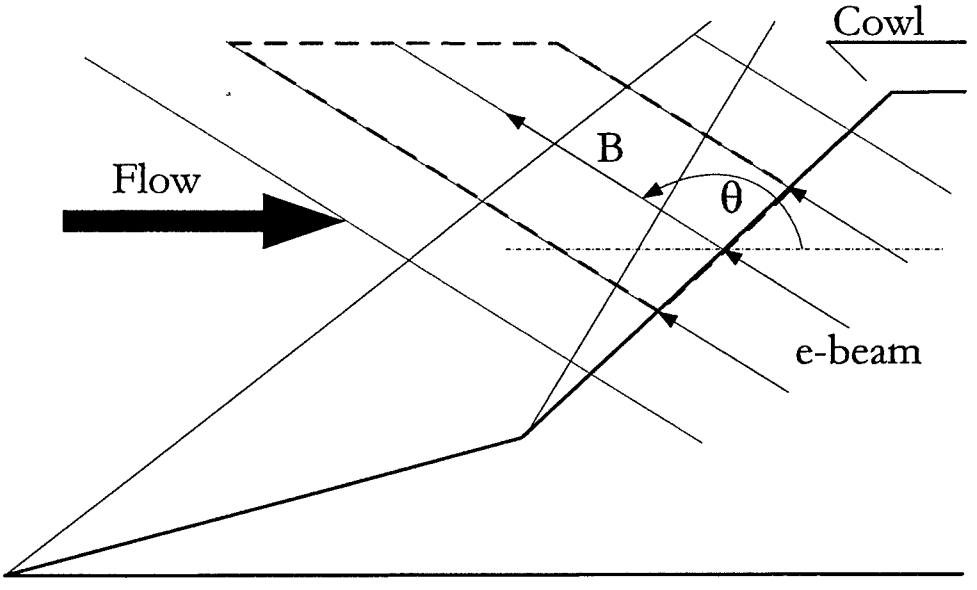

(a) Moving magnetic field and coincident ionizing e-beam

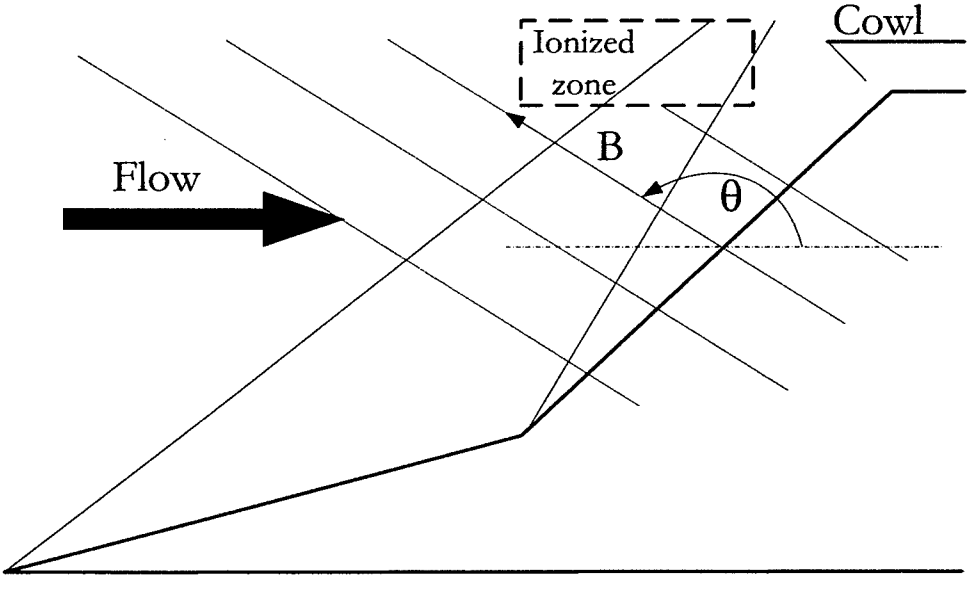

(b) Moving magnetic field and stationary ionized zone

Figure 4.8 Application of magnetic field and ionized region. (a) depicts the coincident ionization region and (b) shows the stationary ionized region.

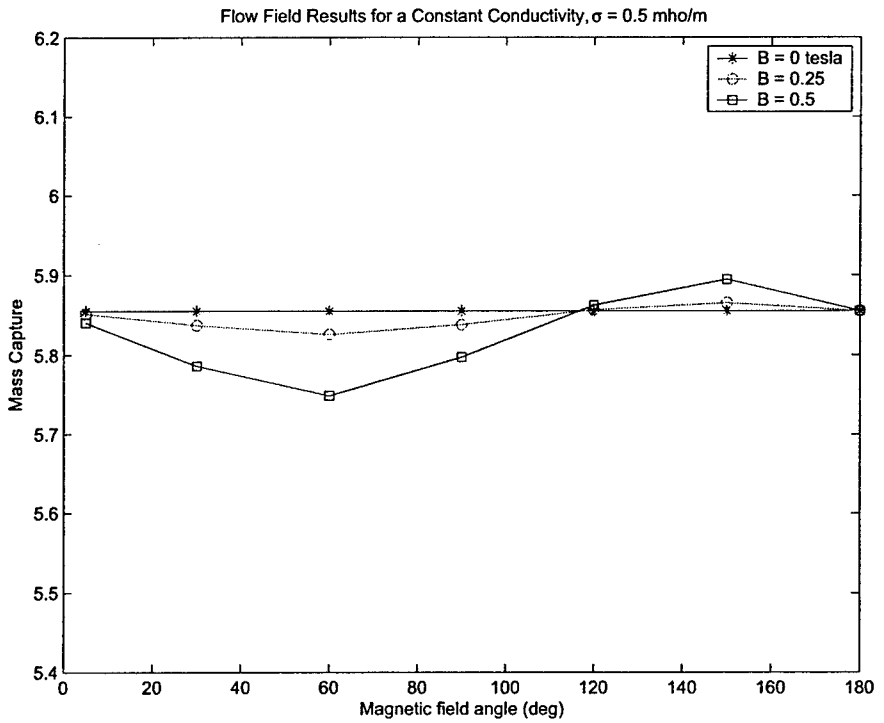

(a) Coincident e-beam ionization

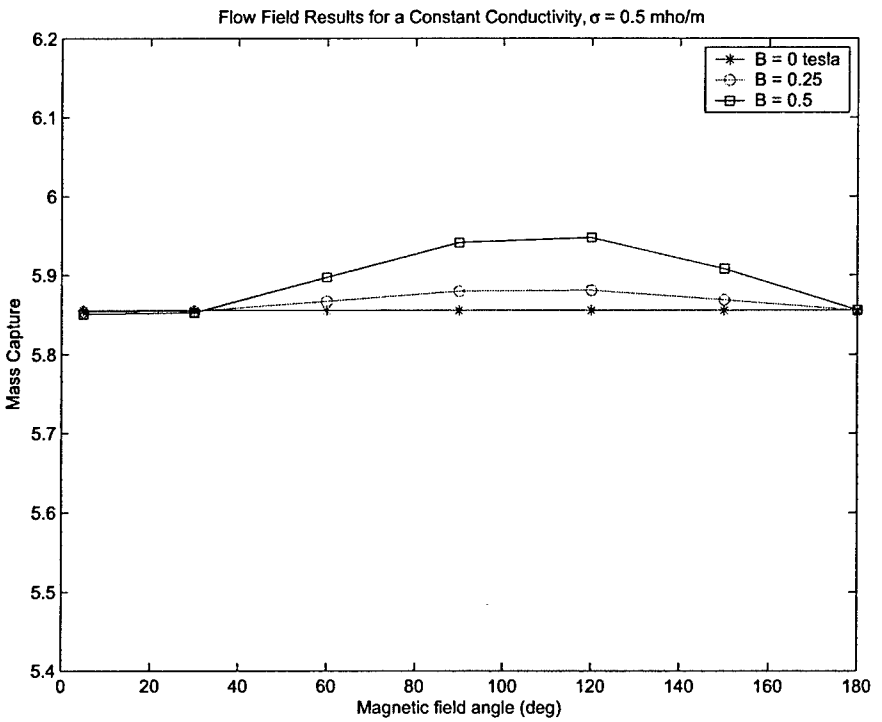

(b) Stationary ionization

Figure 4.9 Mass capture for inlet with conductivity $\sigma = 0.5$ mho/m. Results are shown for (a) coincident ionization and (b) stationary ionization.

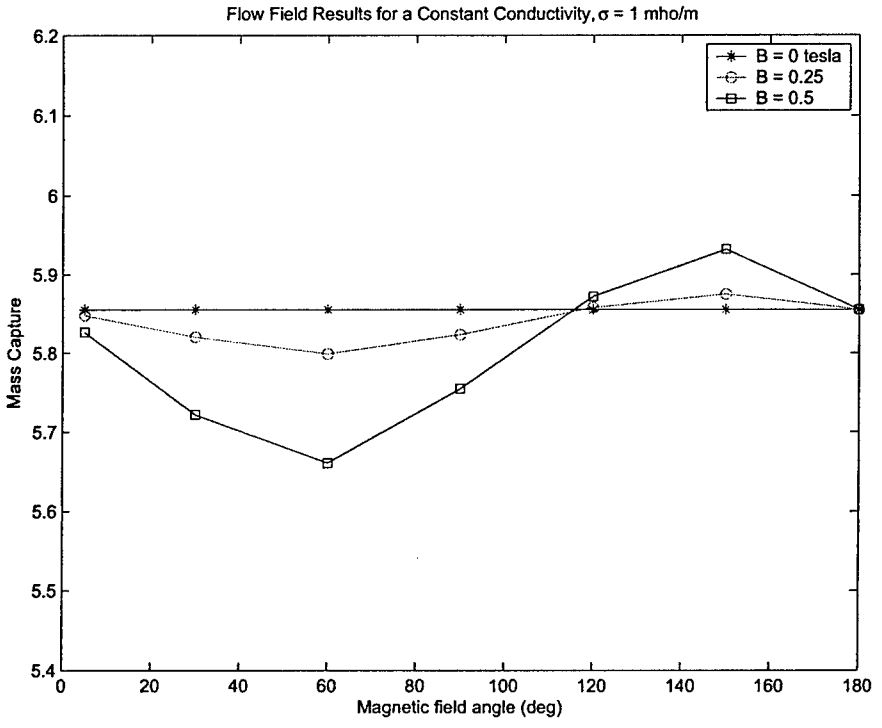

(a) Coincident e-beam ionization

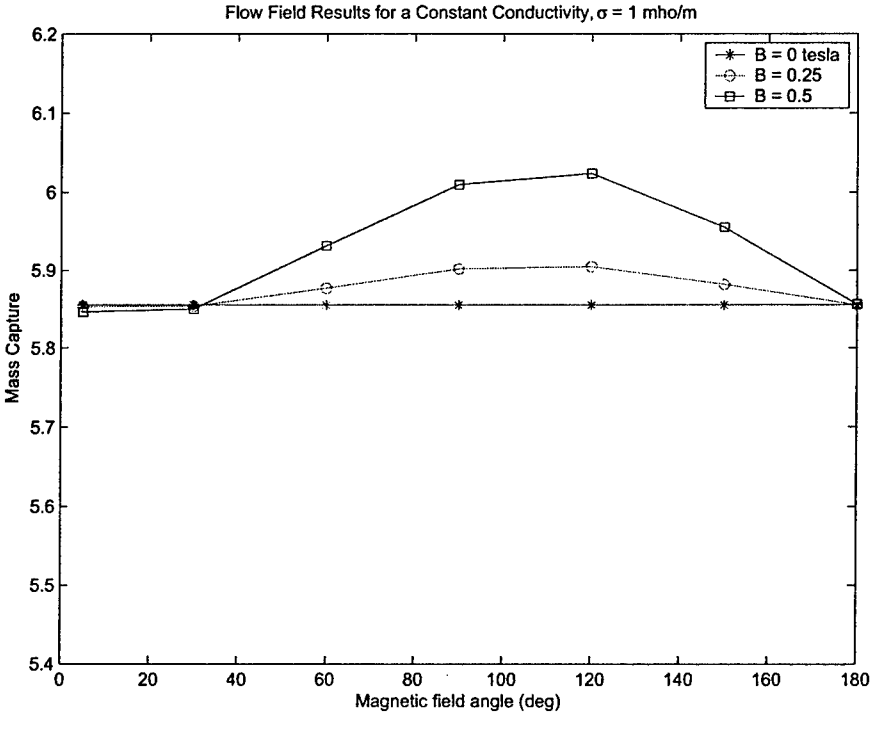

(b) Stationary ionization

Figure 4.10 Mass capture for inlet with conductivity $\sigma = 1.0$ mho/m. Results are shown for (a) coincident ionization and (b) stationary ionization.

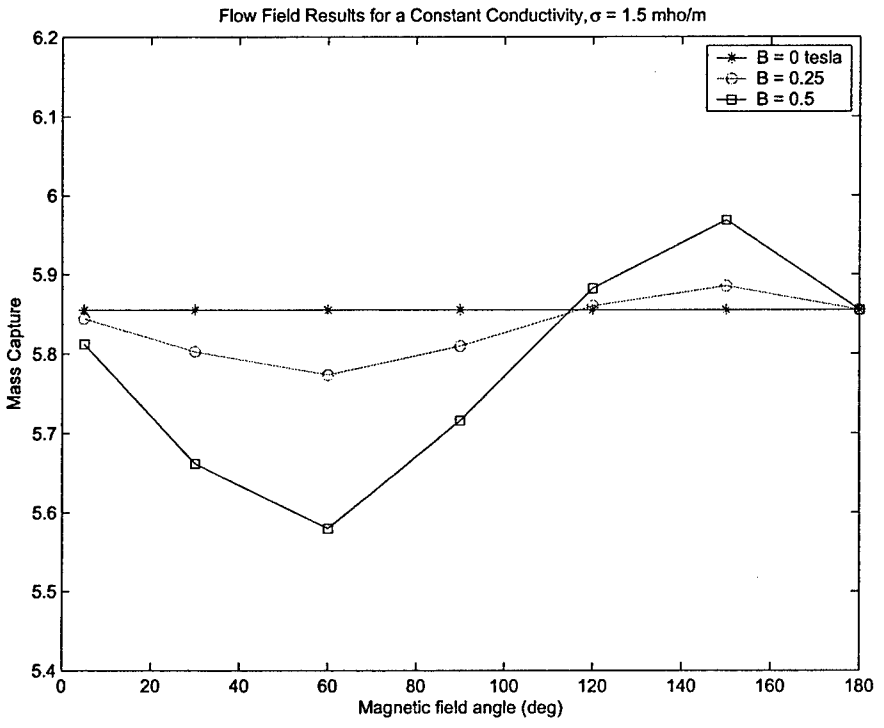

(a) Coincident e-beam ionization

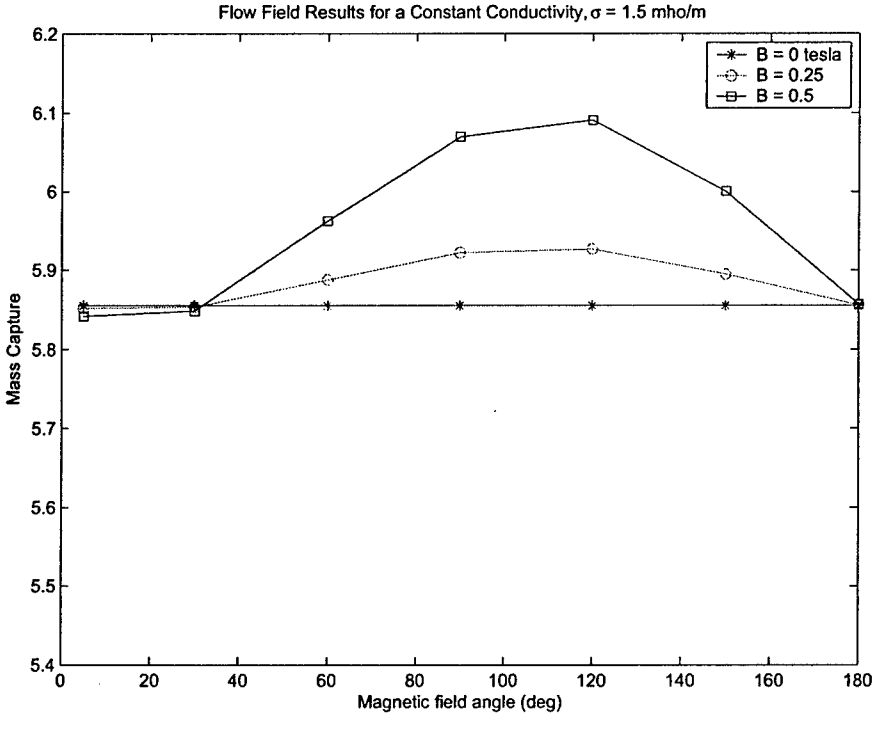

(b) Stationary ionization

Figure 4.11 Mass capture for inlet with conductivity $\sigma = 1.5$ mho/m. Results are shown for (a) coincident ionization and (b) stationary ionization.

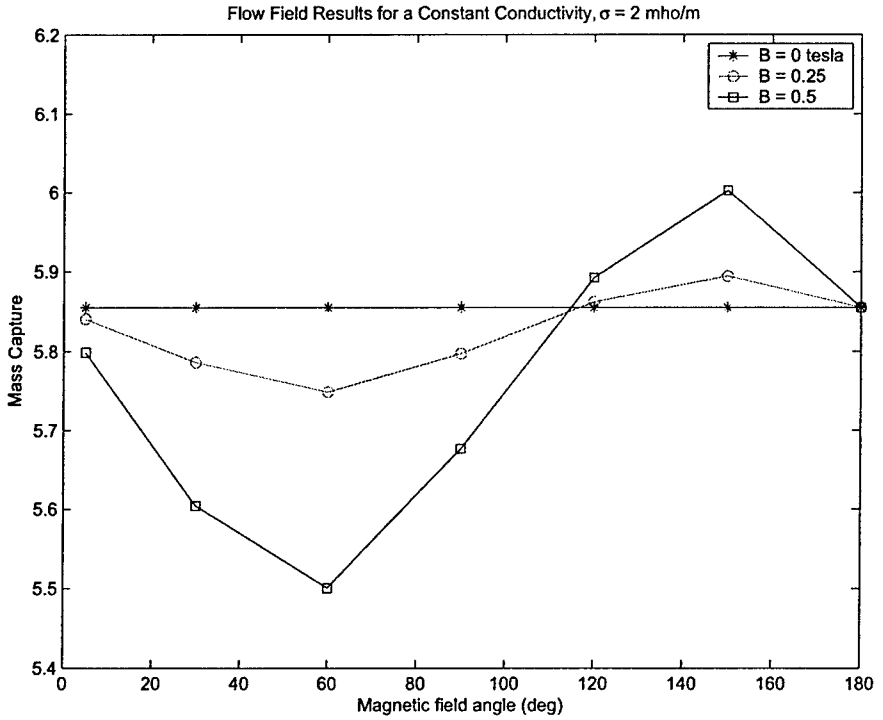

(a) Coincident e-beam ionization

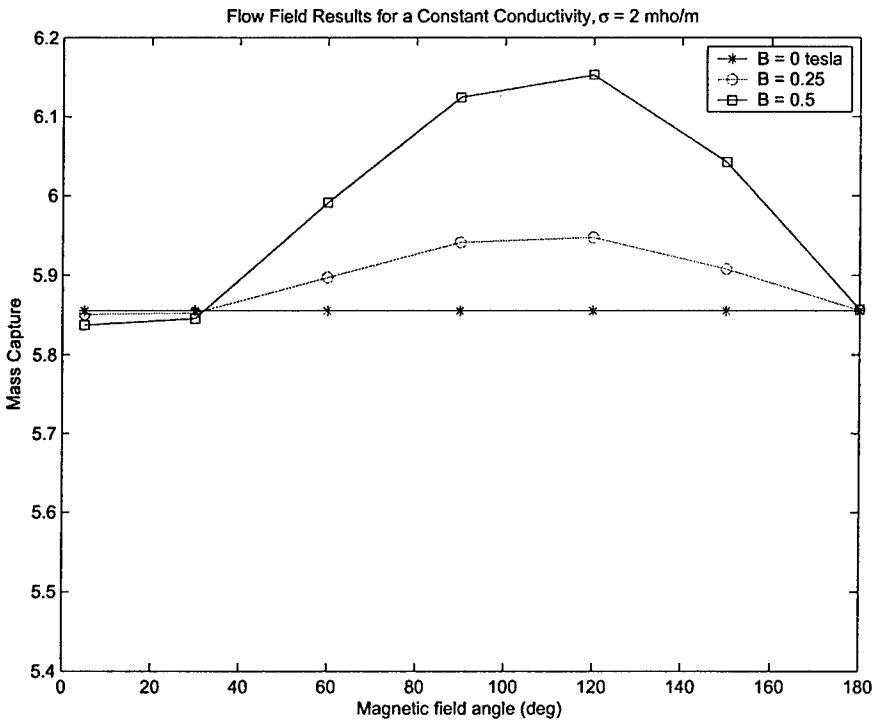

(b) Stationary ionization

Figure 4.12 Mass capture for inlet with conductivity $\sigma = 2.0$ mho/m. Results are shown for (a) coincident ionization and (b) stationary ionization.

Comparing the results of the optimizer with those of the parametric study for the stationary ionized zone we can see a very nice correlation. The spread in the optimized results is not large and is consistent with the parametric study. However in comparing the optimizer results with those of the parametric study in the case of the coincident ionization zone we see a bit of discrepancy. There is a large spread in the values given by the optimizer depending on whether we began the optimization above or below the peak value shown in the parametric study. In order to better understand this result we did another parametric study around the peak value. We limited the study to the $\mathbf{B} = 0.5$ tesla and $\sigma = 2$ mho/m case and varied the magnetic field angle from 120 to 180 degrees. As can be seen in Fig. (4.13) the results of this study show that the curve is not very smooth and this might explain the large range in values given by the optimizer for this case.

To round out the study we decided to try to optimize both the geometry and the magnet field angle. This case may seem redundant in that it would require both actuating surfaces as well as an ionization method and a way to generate the magnetic field, but it is also represents the possibility of fine tuning the magnetic field. Again the off nominal case of $\alpha_1 = 3.0$ deg and $\alpha_2 = 9.0$ deg was used with the initial magnetic field angle of 70 deg. We limited this study to the stationary ionization zone with a conductivity of 2 mho/m and a magnetic field strength of 0.5 tesla, the results of which are shown in Fig. (4.14).

The final configuration for the geometry is very close to that of the optimal mass capture with no MHD source term present, and the final magnetic field angle is consistent with that of the previous case. The results are summarized in table 4.3.

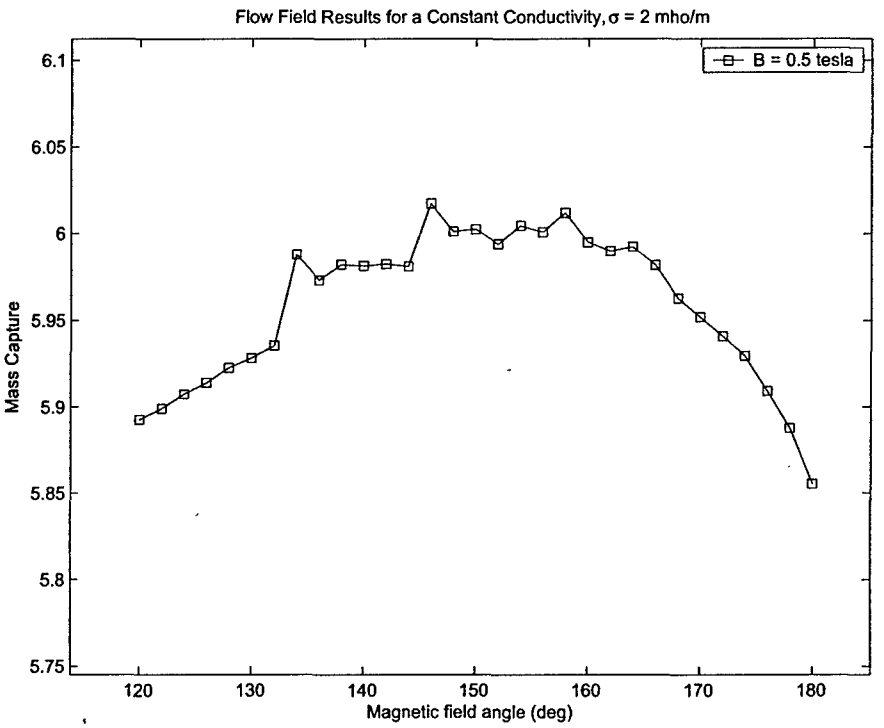

Figure 4.13 Zoom in of peak values for the moving ionization zone.

Table 4.3 Table of optimized geometry and magnetic field angles for stationary ionized zone.

	α_1 (deg)	α_2 (deg)	θ_B (deg)
Initial condition	3.0	9.0	70.0
Optimized value	2.14	9.11	110.5

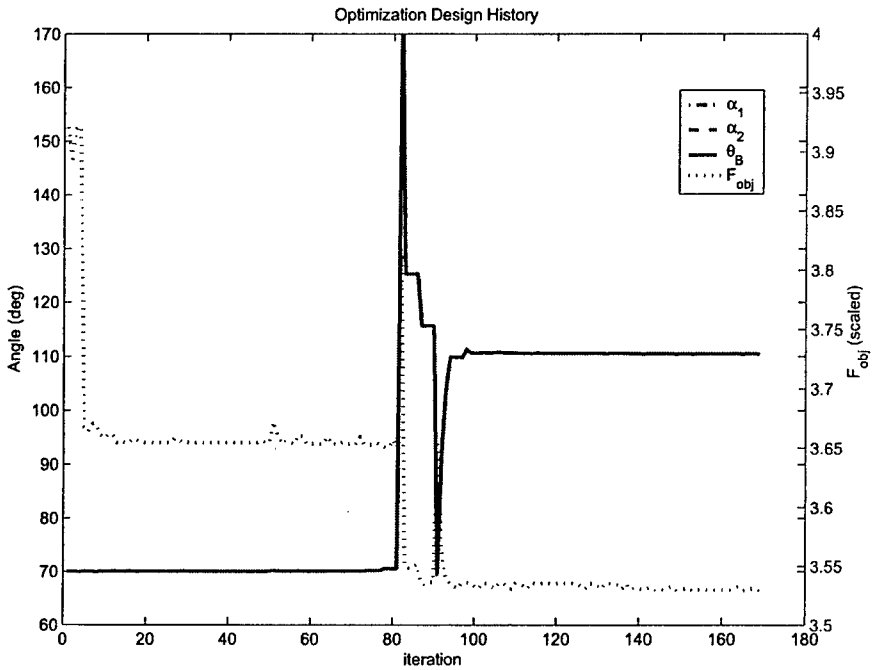

(a) Magnetic field angle history

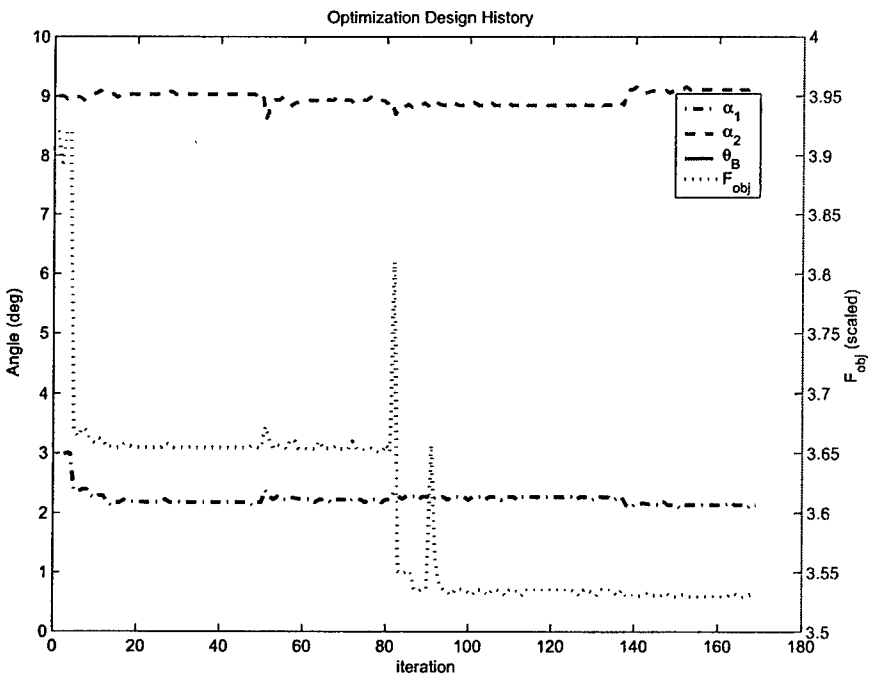

(b) Geometry angle history

Figure 4.14 Optimization design history for (a) the magnetic field angle and (b) geometry angles.

REFERENCES

[1] Korte, J. and Auslender, A., "Optimization of Contoured Hypersonic Scramjet Inlets with a Least-Squares Parabolized Navier-Stokes Procedure," *Computing Systems in Engineering*, Vol. 4, No. 1, 1993, pp. 13–26.

[2] Munipalli, R., Wasawadigi, G., Anderson, D. A., and Wilson, D., "Application of Optimization Techniques in Inlet Design," *AIAA 13th Applied Aerodynamics conference*, June 19-22 1995, AIAA 95-1824.

[3] Sheikin, E. and Kuranov, A., "MHD Controlled Inlet for Scramjet with Various Configurations of Magnetic Field," *AIAA 42nd Aerspace Sciences Meeting and Exhibit*, January 5-8 2004, AIAA 2004-1195.

[4] Shneider, M., Macheret, S., and Miles, R., "Comparative Analysis of MHD and Plasma Methods of Scramjet Inlet Control," *AIAA 41st Aerospace Sciences Meeting and Exhibit*, January 6-9 2003, AIAA 2003-0170.

[5] Macheret, S., Shneider, M., and Miles, R., "Magnetohydrodynamic Control of Hypersonic Flows and Scramjet Inlets Using Electron Beam Ionization," *AIAA Journal*, Vol. 40, No. 1, January 2002.

[6] Macheret, S., Shneider, M., and Miles, R., "External Supersonic Flow and Scramjet Inlet Control by MHD with Electron Beam Ionization," *AIAA 39th Aerospace Sciences Meeting and Exhibit*, January 8-11 2001, AIAA 2001-0492.

[7] Davidson, P., *An Introduction to Magnetohydrodynamics*, Cambridge University Texts in Applied Mathematics, Cambridge University Press, 2001.

[8] Rosa, R. J., *Magnetohydrodynamic Energy Conversion*, McGraw-Hill Book COmpany, 1968.

[9] Miles, R. B., "Flow Control by Energy Addition into High-Speed Air," *AIAA Fluids 2000 Conference*, June 19-22 2000, AIAA 2000-2324.

[10] Macheret, S. O., Shneider, M. N., and Miles, R. B., "Energy-Efficient Generation of Nonequilibrium plasmas and their application to hypersonic MHD systems," *AIAA 4th Weakly Ionized Gases Workshop*, June 11-14 2001, AIAA 2001-2880.

[11] Macheret, S. O., Shneider, M. N., and Miles, R. B., "Potential Performance of Supersonic MHD Power Generators," *AIAA 39th Aerospace Sciences Meeting and Exhibit*, Jan 8-11 2001, AIAA 2001-0795.

[12] Shakhnov, I. and Shcherbakov, V., "Optimization of MHD Generators," *English Translation: Magnetohydrodynamics*, Vol. 2, No. 4, 1966, pp. 29–32.

[13] Carter, C., "The Optimization of a Magnetohydrodynamic Generating Duct," *British Journal of Applied Physics*, Vol. 17, 1966, pp. 863–871.

[14] Kuranov, A., Korabelnicov, A., Kuchinskiy, V., and Sheikin, E., "Fundamental Techniques of the 'AJAX' Concept. Modern State of Research," *AIAA/NAL-NASDA-ISAS 10th International Space Planes and Hypersonic Systems and Technologies Conference*, Apr 24-27 2001, AIAA 2001-1915.

[15] Macheret, S. O., Shneider, M. N., and Miles, R. B., "MHD Power Extraction from Cold Hypersonic Air Flows with External Ionizers," *Journal of Propulsion and Power*, Vol. 18, No. 2, March-April 2002, pp. 424–431.

[16] Kuranov, A. and Sheikin, E., "MHD Control on Hypersonic Aircraft Under 'AJAX' Concept. Possibilites of MHD Generator," *AIAA 40th Aerspace Sciences Meeting and Exhibit*, January 14-17 2002, AIAA 2002-0490.

[17] Kuranov, A. and Sheikin, E., "Magnetohydrodynamic Control on Hypersonic Aircraft Under 'AJAX' Concept," *Journal of Spacecraft and Rockets*, Vol. 40, No. 2, March-April 2003.

[18] Kulkarni, N. V. and Phan, M. Q., "Performance Optimization of a Magnetohydrodynamic Generator at the Scramjet Inlet," *AIAA/AAAF 11th International Spaceplanes and Hypersonic Technologies Conference*, September 2002, AIAA 2002-5121.

[19] Macheret, S. O., Shneider, M. N., and Miles, R. B., "Magnetohydrodynamic and Electrohydrodynamic Control of Hypersonic Flows of Weakly Ionized Plasmas," *AIAA Journal*, Vol. 42, No. 7, July 2004.

[20] Sampath, R. and Zabaras, N., "A functional Optimization Approach to an Inverse Magnetoconvection Problem," *Computer Methods in Applied Mechanics and Engineering*, Vol. 190, 2001, pp. 2063–2097.

[21] Anderson, J. D., *Computational Fluid Dynamics*, McGraw-Hill, Inc., 1995.

[22] Liou, M. and Steffen, C., "A new flux splitting scheme," *Journal of Computational Physics*, Vol. 107, No. 1, July 1993.

[23] Tannehill, J. C., Anderson, D. A., and Pletcher, R. H., *Computational Fluid Mechanics and Heat Transfer*, Series in Computational Methods and Physical Processes in Mechanics and Thermal Sciences, Taylor and Francis Group, 2nd ed., October 1 1997.

[24] Steger, J. L. and Chaussee, D. S., "Generation of Body Fitted Coordinates Using Hyperbolic Partial Differential Equations," *SIAM Journal of Scientific and Statistical Computing*, Vol. 1, No. 4, December 1980, pp. 431–437.

[25] Hanley, P., "Hanley Innovations," http://www.hanleyinnovations.com/.

[26] The MathWorks Inc., *Optimization Toolbox User's Guide*, 2000.

[27] Giles, M. and Pierce, N., "An introduction to the adjoint approach to design," *Flow, Turbulence and Combustion*, Vol. 65, 2000, pp. 393–415.

[28] Jameson, A., "Aerodynamic Design via Control Theory," *Journal of Scientific Computing*, Vol. 3, No. 3, 1988, pp. 233–260.

[29] Abbott, I. H. and Doenhoff, A. E. V., *Theory of Wing Sections*, Dover Publications, 1959.

[30] Currie, I., *Fundamental Mechanics of Fluids*, Marcel Dekker Inc., 3rd ed., 2003.

[31] Giles, M. and Pierce, N., "Analytic adjoint solutions for the quasi-one-dimensional Euler equations," *Journal of Fluid Mechanics*, Vol. 426, 2001, pp. 327–345.

[32] Giles, M. and Pierce, N., "On the properties of solutions of the adjoint Euler equations," *6th ICFD Conference on Numerical Methods for Fluid Dynamics*, 1998.

[33] Giles, M. and Pierce, N., "Adjoint equations in CFD: duality, boundary conditions and solution behaviour," *AIAA Paper*, Vol. 97-1850, 1997, pp. 182–198.

[34] Jameson, A., "Aerodynamic Shape Optimization Using the Adjoint Method," *Lectures at the Von Karman Institute, Brussels*, Febuary 2003.

[35] Jameson, A., Alonso, J. J., Reuther, J. J., Martinelli, L., and Vassberg, J. C., "Aerodynamic shape optimization techniques based on control theory," Fluid Dynamics Conference, 29th, Albuquerque, NM, June 15-18 1998, AIAA 1998-2538.

AFRL-SR-AR-TR-05-

0265

REPORT DOCUMENTATION PAGE

1. REPORT DATE *(DD-MM-YYYY)*	2. REPORT TYPE	3. DATES COVERED *(From - To)*
	Final Report	01 Sep 2004 - 31 May 2005

4. TITLE AND SUBTITLE
Automated Design Optimization for Hypersonic Plasma-Aerodynamics

5a. CONTRACT NUMBER

5b. GRANT NUMBER
FA9550-04-C-0117

5c. PROGRAM ELEMENT NUMBER

6. AUTHOR(S)
Ramakanth Munipalli

5d. PROJECT NUMBER

5e. TASK NUMBER

5f. WORK UNIT NUMBER

7. PERFORMING ORGANIZATION NAME(S) AND ADDRESS(ES)
HyPerComp Inc.
31255 Cedar Valley Drive, Suite 327
Westlake Village CA 91362

8. PERFORMING ORGANIZATION REPORT NUMBER

9. SPONSORING/MONITORING AGENCY NAME(S) AND ADDRESS(ES)
USAF/AFRL
AFOSR
875 North Randolph Street
Arlington VA 22203

NA

10. SPONSOR/MONITOR'S ACRONYM(S)

11. SPONSOR/MONITOR'S REPORT NUMBER(S)

12. DISTRIBUTION/AVAILABILITY STATEMENT

Distribution Statement A. Approved for public release; distribution is unlimited.

13. SUPPLEMENTARY NOTES

14. ABSTRACT

This report is divided into three parts:
In the first part we present our ongoing work on the optimization of an MHD energy by-pass concept. Here we condier the optimization of the power generator and accelerator components individually, and are in the process of a simultaneious optimization of an integrated generator-combustor-accelerator concept in a 2-D sense. We have concentrated our efforts on developing an optimization scheme that couples a flow solver (perfect gas Euler and equilibrium gas N-S) with a Poisson solver for the electric field including Hall effects. The architecture/algorithm of the optimization scheme is such that geometric and/or physical parameters can be optimized for a given set of free-stream conditions and objective function. The objective function was MHD power extracted in the case of a MHD generator, and thrust in the case of an accelerator.
The second part of this report presents some ideas on how to extend this development and the associated real-gas MHD technology at HyPerComp Inc. into a potential Phase-II. We have developed a higher (4th order and beyond) order accurate solver for MHD developed under an AFRL contract.

15. SUBJECT TERMS

16. SECURITY CLASSIFICATION OF:			17. LIMITATION OF ABSTRACT	18. NUMBER OF PAGES	19a. NAME OF RESPONSIBLE PERSON
a. REPORT	b. ABSTRACT	c. THIS PAGE			19b. TELEPHONE NUMBER *(Include area code)*
U	U	U	UU	70	

7-7-05